LIDOCAINE INHIBITION OF CLONED HYPERPOLARIZATION-ACTIVATED CYCLIC NUCLEOTIDE-MODULATED (HCN) CHANNELS

by

RAYMOND HON LEUNG YIP

B.M.L.Sc., The University of British Columbia, 2007

A THESIS SUBMITTED IN PARTIAL FULFILLMENT OF THE REQUIREMENTS FOR THE DEGREE OF

MASTER OF SCIENCE

in

THE FACULTY OF GRADUATE STUDIES

(Physiology)

THE UNIVERSITY OF BRITISH COLUMBIA

(Vancouver)

August 2009

Abstract

Hyperpolarization-activated Cyclic Nucleotide-modulated (HCN) channels underlie the hyperpolarization-activated or "funny" current (I_f or I_h), which is important in regulating excitability in the neurons of the central and peripheral nervous systems and in the conduction tissue of the heart. There are four mammalian isoforms of HCN channels (HCN1-4), each exhibiting different activation and deactivation kinetics. Lidocaine, a local anesthetic and antiarrhythmic drug, has been shown to inhibit HCN-mediated currents in the rabbit sinoatrial (SA) node, which expresses various HCN isoforms. It also inhibits I_h in rat small DRG neurons. Lidocaine has been shown to block Na^+ channels by interacting with the aromatic side chain of a phenylalanine residue in the region lining the channel pore. With the exception of a recent study on rabbit HCN4, this is the first study examining lidocaine inhibition on cloned HCN channels. I hypothesize that lidocaine, in micromolar concentrations, inhibits HCN1 channels from the intracellular side by interacting with amino acid residues lining the channel pore. Lidocaine, at concentrations ranging from 50 to 3200 μM, inhibited mouse HCN1 channels expressed in Chinese hamster ovary (CHO) cells with an IC_{50} of 669 ± 320 μM. The onset of lidocaine action is fast (~6 seconds) and concentration-dependent with maximum inhibition occurring at approximately 20 seconds, and inhibition is partially or completely reversible. The fact that currents does not return completely may be attributed to a phenomenon called current rundown, or to incomplete washout of lidocaine. Extracellular application of the permanently charged derivative of lidocaine, QX-314, did not inhibit the channel, which suggests that lidocaine inhibition, in its charged form, occurs from the intracellular side. A point mutation at the phenylalanine residue does not remove lidocaine inhibition, indicating that this residue is not responsible for interaction with lidocaine. These results support the hypothesis that lidocaine

inhibits HCN1 from the intracellular side, with molecular mechanisms of inhibition yet to be determined.

Table of Contents

List of Figures

List of Symbols and Abbreviations

cAMP	Adenosine 3', 5'-cyclic monophosphate
cGMP	Guanosine 3', 5'-cyclic monophosphate
I_f	Hyperpolarization-activated cation current (in cardiac cells)
I_h	Hyperpolarization-activated cation current (in neurons)
DRG	Dorsal root ganglion
HCN	Hyperpolarization-activated cyclic nucleotide-modulated channel
mV	Millivolt
mM	Millimolar
ms	Millisecond
μM	Micromolar
μl	Microlitre
M	Molar
ZD7288	4-(N-ethyl-N-phenylamino)-1,2-dimethyl-6-(methylamino)-pyrimidinium chloride
QX-314	Lidocaine *n*-ethyl bromide
DMSO	Dimethyl sulfoxide
TEA^+	Tetraethylammonium ion
mRNA	Messenger ribonucleic acid
HEK293	Human embryonic kidney 293 cells
CHO	Chinese hamster ovary cells
WT	Wild-type
°C	Degrees Celsius
Ag	Silver
CO_2	Carbon dioxide

KCl	Potassium chloride
NaCl	Sodium chloride
$MgCl_2$	Magnesium chloride
$CaCl_2$	Calcium chloride
AgCl	Silver chloride
HEPES	4-(2-hydroxyethyl)-1-piperazineethanesulfonic acid
NaOH	Sodium hydroxide
KOH	Potassium hydroxide
ml/min	Millilitres per minute
K-aspartate	L-aspartic acid potassium salt
EGTA	Ethylene glycol-bis(2-aminoethylether)-N,N,N',N'-tetraacetic acid
Mg-ATP	Adenosine 5'-triphosphate magnesium salt
PIP_2	Phosphatidylinositol 4,5-bisphosphate
$M\Omega$	Megaohm
kHz	Kilohertz
SA	Sinoatrial

Acknowledgements

First, I want to sincerely thank my supervisor, Dr. Eric Accili, for his mentorship, support, and patience over the past two years as well as during the two summers I was working in the laboratory as an undergraduate summer student. I am very grateful to him for providing opportunities for me to develop critical and independent thinking, and to learn from my mistakes. His continuous optimism and enthusiasm provided me with confidence and support. I want to thank Dr. Christopher Ahern, member of my supervisory committee, for his help and contribution to my project. His input was invaluable in data analysis and interpretation. I want to thank my other supervisory committee members, Dr. Steven Kehl and Dr. David Mathers, for their time, advice, and feedback. I want to also thank Dr. Stephan Schwarz for taking time out of his busy schedule to serve as an examiner for my defence.

I am grateful to Dr. Damiano Angoli and Vincenzo Macri for teaching me electrophysiology through sharing their expertise and providing technical assistance. Their help allowed me to troubleshoot problems and have a greater understanding on the techniques. I want to extend special thanks to Dr. Damiano Angoli for helping with experimental design and data acquisition. I want to also thank Dr. Andrew Hegle and Christian Peters for taking time to offer advice and feedback for my project as well as proofreading my thesis. I am deeply appreciative towards my fellow lab colleagues Hamed Nazzari, Sarah Chow, Gina Whitaker, and Heather Jackson for their time and patience teaching me molecular biology, cell culture, and other laboratory techniques. Finally, I want to thank my dearest family and friends for their love and support.

Chapter 1: Introduction

Many cellular processes require the transduction of electrical signals to initiate a spontaneous event such as neuron activation and muscle contraction. This signal transduction involves the movement of charges between the inside and the outside of cells. In biological systems, charges are not mobilized in the form of electrons, but rather as inorganic ions such as sodium (Na^+), potassium (K^+), and chloride (Cl^-) ions. However, these ions are unable to permeate the membrane of cells, and require specific proteins on the membrane to assist movement into and out of the cell by lowering the energy barrier posed by the lipid membrane. An interesting membrane protein is the ion channel, which is a transmembrane protein spanning the lipid membrane with access to both the extracellular and intracellular environment. Some ion channels are selective for particular ions, while others are non-selective. Ion channels can be modulated by various factors such as ligand binding and changes in voltage. The extent to which each type of ion channel is affected by these factors provides ion channels with unique physiological functions and differentiates one type of channel from another.

1.1   Hyperpolarization-activated cyclic nucleotide-modulated (HCN) channels

Hyperpolarization-activated cyclic nucleotide-modulated (HCN) channels are unique channels, with opening and closing controlled by both voltage and ligand binding. Their secondary, tertiary, and quaternary structure is based on similarity to voltage-gated potassium or "Kv" channels (Gauss et al., 1998; Ludwig et al., 1998; Santoro et al., 1998). Thus, the channel subunits likely tetramerize to form channels that underlie the hyperpolarization-activated cation current (I_f in cardiac cells or I_h in neurons), which is important in regulating excitability in the

neurons of the central and peripheral nervous systems and in the conduction tissue of the heart.

Like Kv channels, each channel subunit consists of six transmembrane domains or segments (S1-S6) with a pore-forming region between the 5th and 6th transmembrane domains that contains a selectivity filter for Na^+ and K^+ ions (Figure 1.1). The first four transmembrane domains (S1-S4) sense changes in voltage, and control the opening and closing of the channel. The opening and closing of the channel, also known as channel gating, can be modulated by cyclic nucleotides such as cAMP and cGMP, which interact with the cyclic nucleotide binding domain (CNBD) located in the intracellular C-terminus.

Figure 1.1. Predicted topology of a HCN channel subunit. (Biel et al., 2002), used with permission.
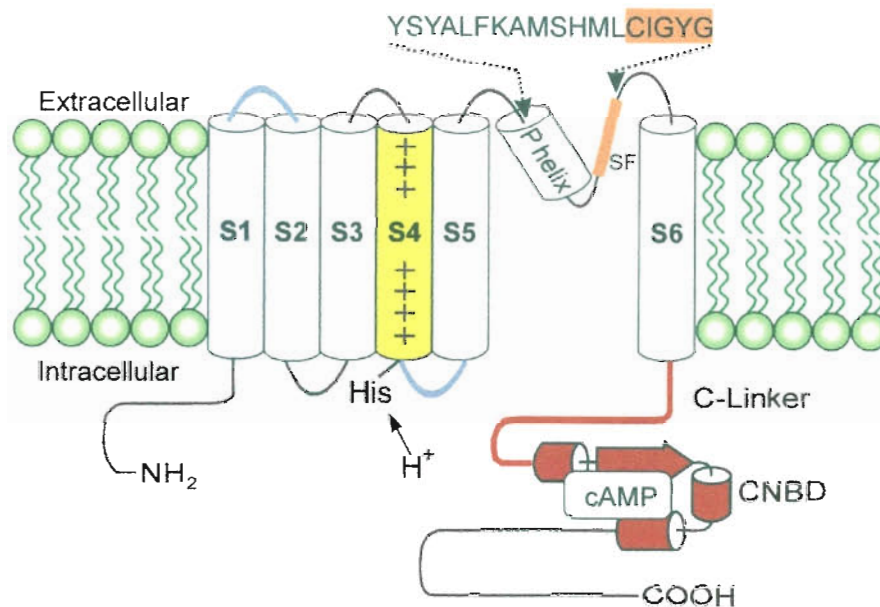
The hyperpolarization-activated cation current is also known as the "funny" current (I_f) because the functional properties of HCN channels are unusual compared to most voltage-gated

2

Na^+ or K^+ channels. HCN channels activate in response to hyperpolarizing voltages, with the midpoint of activation ranging from -73 mV to -92 mV (Accili et al., 2002). I_f is carried by a mixture of K^+ and Na^+ ions with a ratio of approximately 4:1, respectively. In response to hyperpolarized voltages, these channels open to yield an inward current. As positive ions enter the cell, the membrane potential becomes depolarized, and gradually reaches threshold for the next action potential firing. I_h has been described in central and peripheral nervous tissue (Pape, 1996), in which it controls the extent of hyperpolarizations caused by potassium currents and inhibitory inputs (Luthi and McCormick, 1998). I_h is also known to modulate the resting potential and regulate the firing frequency of action potentials (Chan et al., 2004; Ludwig et al., 2003; Nolan et al., 2003; Pape, 1996; Pape and McCormick, 1989). In the heart, I_f contributes to the diastolic depolarization phase of the action potential, which brings the membrane potential from the "undershoot" back to threshold level for the next action potential firing (DiFrancesco, 1993).

There are four mammalian isoforms of HCN channels (HCN1-4), each with unique properties and patterns of distribution in different tissues (Robinson and Siegelbaum, 2003). All four isoforms are expressed in the brain (Ludwig et al., 1998; Santoro et al., 1998). In the sinoatrial node of the heart, HCN4 mRNA is present in the greatest amount, with mRNA of HCN1 and HCN2 also present (Moosmang et al., 2001; Shi et al., 1999). HCN1 activates the fastest among the four isoforms, whereas HCN4 has the slowest time of activation (Altomare et al., 2001). Intracellular cyclic nucleotides, most notably cAMP, can alter the voltage range in which these channels open, with HCN1 being the least responsive (Baruscotti et al., 2005). Thus, within the heart and the brain, the amounts of different HCN isoforms expressed can determine

the kinetics, voltage dependence, and the amount of inward, time-dependent current I_f (Cheng et al., 2007).

1.2   Pharmacology of I_f

Because I_f is important in regulating heart rate as well as action potential firing frequency in neurons, drugs that affect this current can potentially be used to treat patients with irregular heart rates, ischemic heart disease, and neurological diseases. The main goal of HCN channel pharmacological inhibition is to reduce heart rate or firing rate in neurons without compromising other features of the action potential, leading to unwanted side effects. β-blockers and some calcium channel antagonists are examples of agents that can reduce heart rates, but have side effects on the respiratory system and decrease the strength of heart muscle contraction (DiFrancesco and Camm, 2004). In the heart, bradycardic agents are particularly useful in patients with decreased oxygen availability to cardiac tissue and patients with irregular or higher than normal heart rates. Similarly, these agents may be useful to reduce pain in patients with conditions such as neuropathic pain, which may involve HCN channels in the dorsal root ganglion (DRG) neurons contributing to neuronal excitability (Tu et al., 2004). By studying how these drugs affect the channel, important information such as the locations specifically targeted by the drugs can be elucidated. Prior to the cloning of four HCN isoforms from mouse, human, and the sea urchin sperm in the late 1990s (Gauss et al., 1998; Ludwig et al., 1998; Santoro et al., 1998), pharmacological studies could only determine whether specific agents had an effect on I_f in a particular tissue, likely containing a mixture of the isoforms expressed in different amounts. The ability for each HCN isoform to be heterologously expressed in mammalian culture cells

4

allows for experiments examining the effect of drugs on the specific isoforms. The following

section describes the history and properties of two known HCN channel blockers.

1.2.1 ZD7288

ZD7288, a substituted aminopyrimidinium compound, has bradycardic and antianginal

effects (Figure 1.2). It was initially found to block I_f in dissociated guinea-pig sinoatrial node

cells with an IC_{50} of approximately 0.3 µM (BoSmith et al., 1993). Ca^{2+} currents and K^+

currents were also shown to be affected in addition to I_f, albeit to a much lesser extent (BoSmith

et al., 1993). Following the initial characterization of the effects on I_f, ZD7288 was also shown

to inhibit I_h in substantia nigra, the hippocampal CA1 region, thalamocortical neurons and

photoreceptors (Gasparini and DiFrancesco, 1997; Harris and Constanti, 1995). This inhibition

was not found to be frequency- or use-dependent, indicating that inhibition does not accumulate

with each subsequent opening and closing of the channel. The exact mechanism by which

ZD7288 inhibits I_f was not known until studies on cloned HCN channels were performed. In

mammalian HEK293 cells and *Xenopus* oocytes expressing HCN1 cloned from mouse (mHCN1),

ZD7288 enters the channel when it opens, and then becomes trapped in the intracellular side of

the channel when the channel closes (Shin et al., 2001). The inhibition of ZD7288 on the

mHCN1 channel is reversible and is less at more hyperpolarized voltages; however, in another

clone from sea urchin sperm (spHCN), the effect of ZD7288 was not reversible (Shin et al.,

2001). Shin et al. suggest that the differences in amino acid residues in the S6 pore-lining region

between mHCN1 and spHCN may have attributed to the reversibility of inhibition, or lack

thereof. In a recent study, the side chains of two amino acid residues lining the pore region of

HCN2 were suggested to interact with ZD7288 (Cheng et al., 2007) (Figure 1.2). These side

5

chains were speculated to form a hydrophobic cavity for interaction with the aromatic ring of ZD7288. Together, these findings suggest that the pore region of the channel is critical for ZD7288 inhibition.

Figure 1.2. ZD7288 inhibits the HCN2 channel by interacting with hydrophobic side chains of amino acid residues A425 and I432 in the pore-lining region. (Left) Chemical structure of ZD7288. (Right) Aromatic ring of ZD7288 interacts with the hydrophobic pocket formed by the side chains of the amino acid residues predicted to face the central cavity of the channel pore. (Cheng et al., 2007), used with permission.
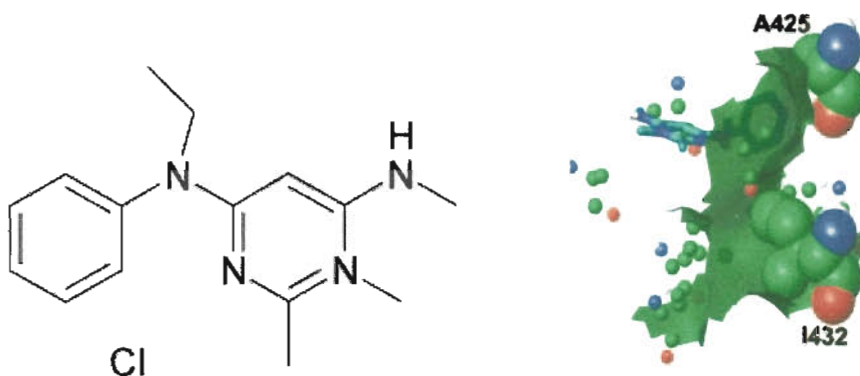
1.2.2 Ivabradine

Ivabradine (S 16257) (Figure 1.3) has been shown to slow down heart rate by inhibiting I_f specifically (DiFrancesco and Camm, 2004). However, side effects such as mild blurred vision and dizziness were observed in patients administered a single 0.2 mg/kg intravenous dose of ivabradine (Camm and Lau, 2003). Blurred vision might have been caused by the effect of ivabradine on I_h in photoreceptors, which express predominantly HCN1 (Barrow and Wu, 2009; Demontis et al., 2002; Moosmang et al., 2001). Ivabradine was initially found to block I_f in

6

rabbit sinoatrial node cells (Thollon et al., 1994). Ivabradine caused minimal prolongation of the action potential duration compared to another bradycardic agent zatebradine (Thollon et al., 1994). Because the reduction in action potential firing frequency was mainly from the reduction in diastolic depolarization, Thollon et al. suggested that ivabradine inhibition was specifically on I_f. Ivabradine block of I_f was use-dependent, with an IC_{50} of 2.8 μM (Bois et al., 1996). Using inside-out and cell-attached patch-clamp configurations, the effect of ivabradine on I_f was found to be similar to that in the whole-cell configuration, suggesting that ivabradine inhibits the channel from the intracellular side (Bois et al., 1996). The authors also showed that ivabradine had minimal effects on the K^+ current responsible for repolarization of the action potential, thus further confirming its bradycardic effect is solely on the pacemaker current I_f. Similar to the studies performed with ZD7288, intensive investigation has been performed with cloned HCN isoforms in trying to decipher the mechanism of inhibition as well as the site(s) of inhibition. Analysis of the effects of ivabradine on cloned mouse HCN1 and human HCN4 channels in HEK293 cells revealed that ivabradine requires the HCN4 channel to open for inhibition, whereas HCN1 channels do not need to be open for inhibition to take place (Bucchi et al., 2006). In contrast to ZD7288, inhibition by ivabradine increases and accumulates with the number of openings and closings of the channel until a certain point when the current ceases to reduce, which may take from 13 seconds with 30 μM up to 90 seconds with 0.3 μM (Bucchi et al., 2002). This property makes ivabradine a good bradycardic agent, as greater inhibition occurs at higher heart rates and reduced effect at lower heart rates. Currently, ivabradine is used clinically as a drug to treat angina pectoris (DiFrancesco and Borer, 2007).

Figure 1.3. Chemical structure of ivabradine (pKa = 8.6).
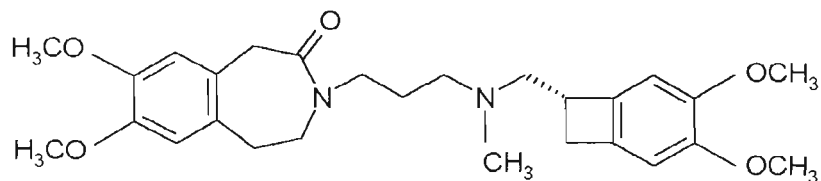
1.3 Local anesthetics

Local anesthetics have been used for more than 150 years to relieve pain. These agents are particularly useful in patients undergoing operations or surgery, and to reduce chronic pain. Early local anesthetics such as cocaine can be found naturally, but can only provide short-duration anesthesia. In addition, the use of cocaine is associated with high toxicity (Arthur and Strichartz, 1987). Local anesthetics with modified chemical structures were synthesized in the early to mid-1900s, and provided longer duration of anesthetic action as well as fewer side effects.

Local anesthetics are characterized by particular chemical structures. All have three chemical moieties that play important functional roles, as well as separating one from another: a lipophilic (aromatic) end, a hydrophilic (amine) end, and a linker between the two ends (Heavner, 2007). The linker can be either an aminoester group, or an aminoamide group. Early local anesthetics such as cocaine and procaine have an ester group as the linker, and are called ester-type local anesthetics. Local anesthetics such as lidocaine that were later synthesized in the early to mid-1900s have an amide group as the linker, and are called amide-type local anesthetics. The amine end is usually a tertiary amine that can be protonated (charged) or remain neutral (uncharged), depending on the pKa of the compound. Local anesthetics, in the uncharged form, move through the lipid membrane and into the cell, then block sodium channels from the

intracellular side (Hille, 1977a). Thus, the relative proportion of charged versus uncharged form of the compound can control the speed of block onset.

Local anesthetics act in part by blocking nociceptive stimuli and transmission to the brain from various regions of the body. Local anesthetics act on the cell membrane, and are well known for their reversible, inhibitory effect on voltage-gated Na^+ channels resulting in block of action potential propagation responsible for nerve conduction in both central and peripheral nerve pathways (Butterworth and Strichartz, 1990). Local anesthetics can also target cardiac cells by affecting permeability of cardiac Na^+ channels (Bean et al., 1983). However, local anesthetics are not necessarily specific Na^+ channel blockers, but may have effects on voltage-gated K^+ channels, voltage-insensitive K^+ channels, two-pore domain K^+ selective channels, and many other membrane-associated proteins (Kindler and Yost, 2005; Komai and McDowell, 2001; Olschewski et al., 1998). The non-specificity in local anesthetic action and its interaction with various channels known to contribute to the action potential lead to the possibility that HCN channels are also targeted.

Because I_h has been shown in peripheral nerves and DRG neurons (Grafe et al., 1997; Mayer and Westbrook, 1983; Takigawa et al., 1998), it is possible that block of action potential generation and propagation in peripheral nerves by local anesthetics may be due to block of I_h. A recent study has demonstrated that HCN1 knockout mice experience less cold allodynia in a neuropathic pain model (Momin et al., 2008). Also, I_h is composed of mainly HCN1-mediated currents in large-diameter and fast-conducting medium-diameter neurons (Momin et al., 2008). Thus, I_h may play a significant role in the generation of action potentials and transmission of pain signals. One study examined the effect of three local anesthetics on I_h in rat small dorsal root ganglion (DRG) neurons. Bupivacaine, lidocaine, and mepivacaine all have significant and

reversible effects on I_h when applied extracellularly, with IC_{50} of 55, 99, 190 µM respectively (Bischoff et al., 2003). It is likely that mechanism of drug action on peripheral nerves by local anesthetics can be partly attributed to block in I_h.

1.3.1 Lidocaine

Lidocaine is a common local anesthetic and a class Ib antiarrhythmic drug that is known to inhibit conductance of Na^+ channels with possible effects on K^+ channels (Hille, 2001; Olschewski et al., 1996). Lidocaine can reduce heart rates (Goodman et al., 2001), and is contraindicated in patients with heart failure and bradycardia when administered intravenously (Harrison and Collinsworth, 1974). Lidocaine's effects both as an antiarrhythmic and a local anesthetic mostly involve lowering sodium permeability by inhibiting voltage-gated Na^+ channels, in order to slow heart rates and reduce pain. The concentration needed to have significant effects on cardiac Na^+ channels is approximately 15 to 30 µM (Bean et al., 1983; Grant et al., 1980; Hondeghem and Katzung, 1977). Therapeutic concentrations used to treat heart conditions such as arrhythmias range from approximately 5 to 20 µM (Burashnikov et al., 2007). In nerves, however, the concentration needed to have significant effects on Na^+ channels is approximately 100 to 250 µM (Hille, 1977b). Clinically, lidocaine patches applied to the skin have a concentration of 5% or approximately 200 mM (Galer et al., 1999).

Similar to action on Na^+ channels, lidocaine has been shown to inhibit I_h in nerves and I_f in the heart. As described above, lidocaine inhibits I_h in rat small DRG neurons, with an IC_{50} of 99 µM (Rocchetti et al., 1999). In rabbit sinoatrial myocytes, lidocaine has been shown to inhibit I_f in a concentration-dependent manner, with an IC_{50} of approximately 38 µM and up to

70% reduction in current by 100 μM of lidocaine (Rocchetti et al., 1999). Thus, the

antiarrhythmic effect of lidocaine can be attributed in part to its action on I_f.

A recent study showed effects of various antiarrhythmic drugs on rabbit HCN4 channels

expressed in HEK293 cells. In low K^+ (Tyrode) extracellular solution, lidocaine inhibited

HCN4-mediated currents at -70 mV with an IC_{50} of 276 μM (Tamura et al., 2009). Although

lidocaine, at 30 μM, appeared to inhibit I_f to a greater extent at more hyperpolarized potentials,

this was not significantly different from control. Unlike the study examining lidocaine inhibition

of I_f in rabbit SA myocytes (Rocchetti et al., 1999), Tamura et al. evaluated lidocaine inhibition

only at a potential of -70 mV where channels were not fully-activated. Finally, it was not clear

to what extent current rundown contributed to the inhibition observed by Tamura et al.

Therefore, a number of issues remain to be resolved with respect to the mechanism of lidocaine

block of HCN channels as well as whether inhibition by this drug is similar among HCN

isoforms.

Lidocaine has been shown to block Na^+ channels by binding to aromatic side chains of

amino acid residues lining the pore, specifically phenylalanine (Ahern et al., 2008). This

interaction involves the cation from the ionized amine group of lidocaine and the π-electrons

from the aromatic ring of phenylalanine (Ahern et al., 2008) (Figure 1.4). At a pH lower than the

pKa of 7.9, most lidocaine molecules acquire a proton and become charged (Figure 1.5). At a

physiological pH of 7.4, approximately 25 % of lidocaine molecules remain uncharged. In

extracellular solution, uncharged lidocaine molecules diffuse through the cell membrane to the

inside of the cell, and become the active form once protonated (Hille, 1977a). Thus, most of the

intracellular lidocaine can readily bind to the suspected binding site in the channel pore. This

claim can be supported by experiments showing intracellular effects on I_h by the quaternary,

11

permanently charged derivative of lidocaine, QX-314, in guinea pig hippocampal CA1 pyramidal cells and Cajal-Retzius cells in the neocortex of rat neonates (Kilb and Luhmann, 2000; Perkins and Wong, 1995). In all four mouse HCN isoforms, phenylalanine residues are found in the pore-lining sixth transmembrane domain (S6) region: amino acid 378 in mHCN1, amino acid 431 in mHCN2, amino acid 341 in mHCN3, and amino acid 509 in mHCN4 (Figure 1.6). With amino acids having aromatic side chains lining the pore of HCN channels, it is reasonable to propose that lidocaine inhibits HCN channels via a cation-π interaction.

Figure 1.4. The aromatic ring of Phe1579 in the S6 region of Domain IV in Na$_v$ 1.4 is responsible for cation-π interaction with the charged amine group of lidocaine. (Ahern et al., 2008), used with permission.
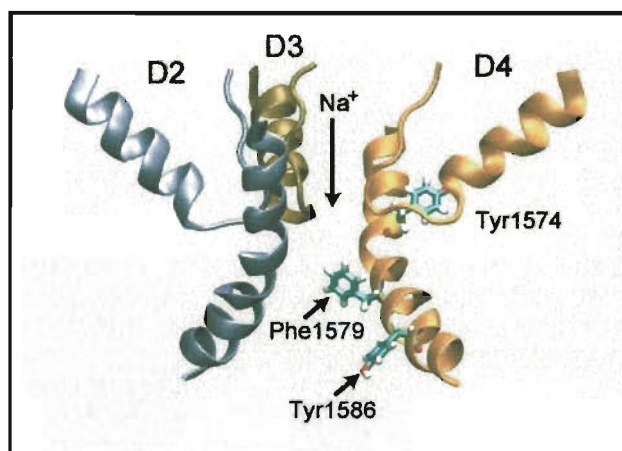
Figure 1.5. Chemical structure of lidocaine (pKa = 7.9).
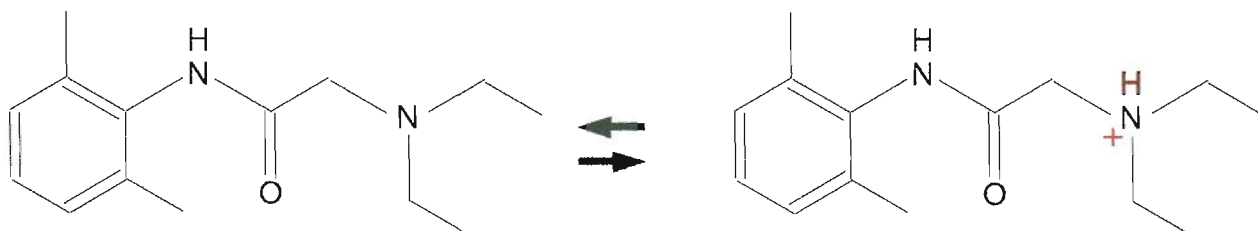
Figure 1.6. Phenylalanine is conserved in the S6 pore-lining region across the four mammalian HCN isoforms.

It is important to know whether lidocaine, which is an important therapeutic agent and is used extensively in clinical situations, inhibits individual HCN isoforms differently. Individual tissues express different amounts and combinations of HCN isoforms. By examining the effects of lidocaine on each cloned HCN isoform, the relative sensitivity of each body tissue to lidocaine can be estimated, based on the predominant isoforms expressed by each tissue. Moreover, details about possible binding sites on the each channel isoform to lidocaine can be elucidated by comparing the actions on each isoform. This information can be beneficial in the development of more specific therapeutic strategies for treating patients with conditions such as arrhythmia, and for reducing unwanted side effects such as bradycardia.

1.4 Summary

HCN channels underlie the hyperpolarization-activated cation current, which is important in controlling the "pace" of many physiological functions. Abnormalities in channel function can result in neuronal and heart diseases. These can be remedied by the use of agents that control or inhibit this current specifically. Many studies have been performed on other types of ion channels that contribute to pacemaking such as voltage-gated Na^+ and K^+ channels, yielding valuable information in treating diseases associated with malfunction of these channels. However, the role of HCN channels and the pacemaker current should not be underestimated. Even though use of many clinical drugs, such as local anesthetics, may be deemed safe, these drugs may have potential side effects by targeting other molecules such as the pacemaker channels. It has been shown that lidocaine, a local anesthetic, has an inhibitory effect on the pacemaker current under clinically relevant concentrations. Inhibiting I_h may also contribute to the wanted effects such as reducing pain in achieving anesthesia. Thus, it is important to

understand more about the blocking mechanism so that safer drugs can be designed, and also to understand how the structure of the channel contributes to the inhibitory action.

Based on the background presented, it seems reasonable to test whether lidocaine inhibits HCN1 channels, and if the mechanism of block may involve the binding of the drug to an intracellular site along the S6 segment. The objectives of this thesis are to address the effects of lidocaine on I_f and channel kinetics of cloned HCN1 channels, and to compare our findings with studies examining effects of lidocaine on native I_f as well as on Na^+ and K^+ channels. I will first present the hypothesis with specific aims used to support or disprove the hypothesis. Details of each experiment are described in the following Materials and Methods chapter. Findings in this study are then presented, in the order of the specific aims, followed by discussion and interpretation of the results.

1.5   Hypothesis and specific aims

<u>Hypothesis</u>

Lidocaine, in micromolar concentrations, inhibits HCN1 channels from the intracellular side by interacting with amino acid residues lining the channel pore.

<u>Specific aims</u>

1) To determine whether lidocaine inhibits the HCN1 channel in micromolar concentrations and to construct a concentration-response relationship.

2) To determine whether lidocaine affects the steady-state activation and rates of activation and deactivation of the channel.

3) To determine whether the permanently charged derivative of lidocaine (QX-314), applied in the extracellular solution, inhibits the HCN1 channel.

4) To identify residues in the S6 pore-lining region of the channel responsible for lidocaine interaction and inhibition.

Chapter 2: Materials and Methods

2.1 Solutions and chemicals

Low K^+ extracellular solution consisted of 5.4 mM KCl, 135 mM NaCl, 0.5 mM $MgCl_2$,

1.8 mM $CaCl_2$, 5 mM HEPES, pH 7.4 (NaOH). High K^+ solution or control solution, used for

recordings to maximize current amplitude, consisted of 135 mM KCl, 5.4 mM NaCl, 0.5 mM

$MgCl_2$, 1.8 mM $CaCl_2$, 5 mM HEPES, pH 7.4 (KOH). Intracellular-like solution filled into the

patch pipettes contained 130 mM K-aspartate, 10 mM NaCl, 0.5 mM $MgCl_2$, 5 mM HEPES, 1

mM EGTA, 2 mM Mg-ATP, 2 mM creatine phosphate, 1 mM cAMP, 20 μM PIP_2, pH 7.4

(KOH). Certain compounds such as Mg-ATP, cAMP, and PIP_2 were included in the intracellular

solution to minimize the effects of current rundown, which is known to shift the voltage-

dependence of activation in the hyperpolarized direction (Pian et al., 2006). Current rundown is

described in detail in the discussion section on page 63. 2 mM Mg-ATP shifts the midpoint of

activation ($V_{1/2}$) of HCN2 in the depolarized direction by 9.5 mV (Pian et al., 2006). HCN1 is

less responsive to cAMP compared to HCN2 and HCN4 (Accili et al., 2002), and 1 μM cAMP

only shifts $V_{1/2}$ by 2 mV in the depolarized direction (Santoro et al., 1998). Using the

experimental system and procedures in our laboratory, 1 mM cAMP was found to shift $V_{1/2}$ in

the depolarized direction by approximately 10 mV in HCN2 (Proenza et al., 2002). For cAMP to

have an effect against current rundown, a concentration of 1 mM was used. Moreover, a

depolarizing shift in $V_{1/2}$ of approximately 15 mV was observed with 25 μM PIP_2 in HCN2 (Pian

et al., 2006). This intracellular-like solution was first made in 1 mL aliquots stored at -20°C. On

the day of the experiment, one tube was thawed and dispensed into a syringe. The syringe with

the intracellular solution was placed in room temperature for at least 15 minutes before use.

17

Lidocaine (Sigma-Aldrich) was dissolved in DMSO and made into 1 mL of 100 mM and 500 mM stocks stored at 4°C. Lidocaine was diluted to the desired concentrations with high K^+ solution on the day of the experiment, and was placed in room temperature for at least 15 minutes prior to use. The 100 mM stock was used to make final concentrations up to 100 μM, and the 500 mM stock was used to make final concentrations higher than 100 μM. Stock solutions of higher concentrations were not used because lidocaine did not completely dissolve in stock solutions higher than 500 mM. This procedure ensured that the % DMSO in the recording solution was kept to a minimum. Use of lidocaine hydrochloride may have provided a better indication of lidocaine inhibition, as this form is used clinically and is soluble in water. It seems possible that the structure of lidocaine might differ when dissolved in DMSO or water. QX-314 (Sigma-Aldrich) was dissolved in water, and made into 1 mL of 20 mM stock stored at 4°C. QX-314 was diluted to the desired concentration with high K^+ solution on the day of the experiment, and was placed in room temperature for at least 15 minutes prior to use.

2.2   Site-directed mutagenesis

Three mutants, each with single amino acid residue substitutions in the pore-lining S6 region, were made to determine whether lidocaine inhibition involved interaction with these residues. Substitution of phenylalanine at position 378 with alanine was based on homology to a phenylalanine located in the S6 pore-lining region of the fourth homologous domain (D4) in $Na_v1.4$, at which lidocaine, in its charged form, interacted with π electrons of the aromatic ring (Ahern et al., 2008). Na^+ channels were chosen for comparison, as lidocaine inhibition on Na^+ channels have been studied more extensively compared to K^+ channels. Also, Na^+ channels possess similar structure compared to HCN channels in that the S6 region lines the channel pore.

The A372G and V379A mutations were made based on the fact that the side chains from these two amino acid residues are known to form a hydrophobic cavity for the phenyl ring of ZD7288, a known HCN channel blocker (Cheng et al., 2007). There is a phenyl ring present in lidocaine which could occupy the hydrophobic cavity.

Site-directed mutagenesis was performed to produce point mutations at these three sites. Mutant channels were generated by polymerase chain reaction using oligonucleotide primers (synthesized by Integrated DNA Technologies) encoding the mutation of interest using the QuikChange site-directed mutagenesis kit (Stratagene, La Jolla, CA). All mutations were verified by DNA sequencing (Nucleic Acid Protein Service Unit, University of British Columbia).

2.3 Cell culture and transfection

The mammalian culture cells used were CHO-K1 cells (American Type Culture Collection, Manassas, VA), maintained in Ham's F-12 medium (Invitrogen, Ontario, Canada) supplemented with 50 µg/ml penicillin/streptomycin (Invitrogen) and 10% fetal bovine serum (Invitrogen). Cells were grown on glass coverslips (22 x 22 mm) in 35 mm dishes at 37°C with 5% CO_2. Transfection of mammalian expression vectors encoding mouse HCN1 (a kind gift from Dr. Martin Biel, University of Munich) or HCN1 mutant channels generated (1 µg per dish) was performed using the FuGene6 transfection reagent (Roche Diagnostics, Quebec, Canada) according to manufacturer's protocols. The DNA plasmid encoding Green Fluorescent Protein (GFP) was co-transfected for visualization of transfected cells.

19

2.4 Electrophysiological recordings

Approximately 24 to 48 hours post-transfection, a small piece of coverslip was placed into the recording chamber (180 μl volume) on the stage of an inverted microscope. The recording chamber was perfused with low K^+ extracellular solution at a constant rate of 0.5 - 1.0 ml/min. The voltage and current were recorded using a borosilicate glass electrode (Sutter Instruments Co., CA) filled with an intracellular-like solution. The patch pipettes had a resistance of 2.0 - 5.0 MΩ. An Ag-AgCl ground wire was connected to the bath solution by a 3M KCl agar bridge. All currents were measured in the whole-cell configuration. A gigaohm seal between the tip and the cell membrane and rupturing of the membrane patch were obtained via manual suction. The recording chamber (extracellular) solution was changed to high K^+ solution after rupturing of the membrane patch. After one minute of complete perfusion of the new solution, voltage protocols were applied and currents were recorded using an Axopatch 200B amplifier and Clampex software (Axon Instruments Inc., Foster City, CA). Data were sampled at 1 kHz, filtered at 2 kHz, and analyzed using Clampfit (Molecular Devices, CA) and Origin (Microcal, MA) software. Data should have been sampled at least two times the filter -3 dB frequency, as suggested by the Nyquist Sampling Theorem. Despite sampling at a lower frequency, data in this study were still reliable and currents could be accurately quantified. Currents were not leak subtracted, and capacitance compensation was not used. All experiments were performed at room temperature.

2.5 Protocols and data acquisition

The whole-cell patch-clamp method was used to measure currents, which were elicited by applying a series of hyperpolarizing pulses from a holding potential of -35 mV. Micromolar

concentrations of lidocaine were added to cells to determine whether HCN-mediated currents (I_f) were reduced, similar to studies examining effects on I_h in rat small DRG neurons (Bischoff et al., 2003) and on I_f in rabbit SA myocytes (Rocchetti et al., 1999). Currents were recorded before, during, and after lidocaine application to the extracellular side of the membrane. Cells in which current return was partial or complete were chosen for analysis.

To determine whether the mechanism of lidocaine block was by gradually blocking ions passing through the channel pore, a protocol consisting of activation and deactivation steps was applied every 6 seconds (1/6 Hz) until reaching steady-state inhibition, followed by washout of the drug. The duration of the activation step varied from 800 to 1000 ms in order for activation currents to reach steady-state, and the duration of the deactivation step was 450 ms. This protocol was used to test whether lidocaine, when delivered directly onto the cell under study via a fast-step perfusion system (Warner Instruments, CT), caused reduction in current amplitude, which could accumulate until steady-state inhibition was reached. This protocol was used to generate a time course showing onset of inhibition and current return. I_f amplitude was calculated as the difference between the steady-state current and the instantaneous current (Figure 2.1). Lidocaine inhibition was expressed as percent of I_f reduction observed during steady-state inhibition relative to control or prior to lidocaine addition. Percent I_f reduction caused by 200 µM lidocaine was examined at hyperpolarizing potentials of -85 mV, -100 mV, and -110 mV.

Inhibition by lidocaine at concentrations of 50, 100, 200, 400, 800, 1600, and 3200 µM was quantified by the percent I_f reduction elicited by the +30 mV deactivation step. I_f amplitude was calculated as the difference between the peak current and the steady-state current (Figure 2.1). The percent I_f reduction was determined by the difference between I_f at steady-state inhibition

21

and I_f prior to lidocaine addition. Similar protocols were used for experiments on the HCN1 F378A mutant, with the exception that the duration of the activation step varied from 1000 to 1500 ms and the duration of the deactivation step was 5000 ms for currents to reach steady-state. Because of the prolonged duration in deactivation, trains of activation/deactivation steps were applied every 8 seconds (1/8 Hz). Controls were performed using high K^+ solution containing % DMSO equivalent to that in the lidocaine solution.

Figure 2.1. I_f calculation from current traces elicited by -130 mV and +30 mV. (Top) At -130 mV, I_f amplitude was calculated as the difference between the steady-state current and the instantaneous current (I_{inst}). (Bottom) At +30 mV, I_f amplitude was calculated as the difference between the peak current and the steady-state current.
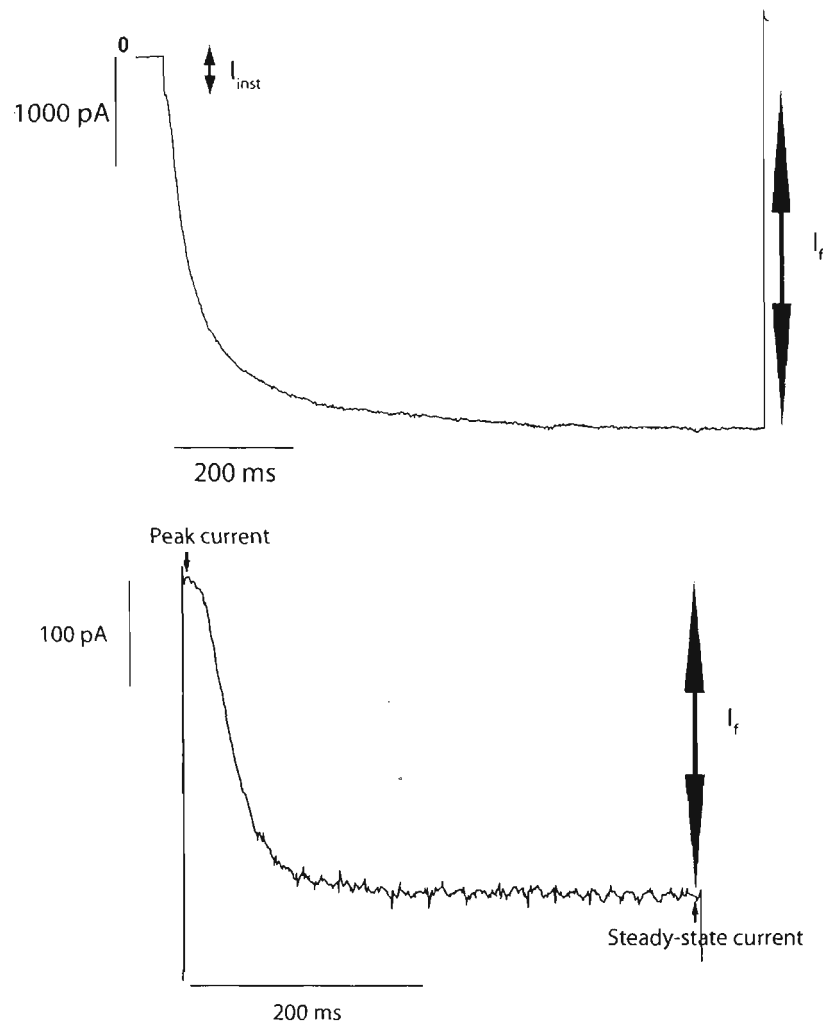
The effects of QX-314 were examined using the same experimental protocol when delivered extracellularly at a concentration of 500 μM. This concentration was at least 2 to 5-fold lower compared to intracellular QX-314 concentrations used to inhibit I_h in guinea pig hippocampal CA1 pyramidal cells and Cajal-Retzius cells in the neocortex of rat neonates (Kilb and Luhmann, 2000; Perkins and Wong, 1995). Because the objective of this experiment was to

23

determine whether lidocaine, in its charged form, interacting with extracellular site(s), the QX-314 concentration chosen was within the range of lidocaine concentrations known to have substantial inhibition on I_f.

Voltage-dependence of activation was determined from tail currents at +30 mV following test pulses ranging from -150 mV to -50 mV in +20 mV steps, with 1800 ms duration for the initial step and an additional 1800 ms for each subsequent step to ensure currents reached steady-state. A 100 ms pulse to +5 mV after the +30 mV step was included to ensure complete channel deactivation. For the F378A mutant, voltage-dependence of activation was determined from tail currents at -35 mV following the same set of test pulses, with 1500 ms duration for the initial step and an additional 500 ms for each subsequent step.

2.6   Data analysis

All data are presented as mean ± standard error of the mean (SEM) (n = number of cells), except parameters generated by fitting the data points using a nonlinear least-squares procedure such as those in the concentration-response curve, which are presented as mean ± standard error (SE). Paired student's t-test was used for statistical comparisons between values from control and a specific lidocaine concentration tested on the same cell, and was not used to assess multi-group differences. Multi-group differences comparing lidocaine inhibition at various concentrations were assessed by one-way analysis of variance (ANOVA), with *post hoc* analysis of individual means using Tukey multiple comparison test to determine which of the means were significantly different. A p-value of less than 0.05 was deemed statistically significant. Curve fitting and generation of bar graphs were performed using Origin software (Microcal, MA), and

statistical analysis such as student's t-test and analysis of variance were performed using GraphPad Prism version 4.0 software (San Diego, CA).

Voltage-dependence of inhibition

$K_{1/2}$ values, or binding constants of lidocaine, at -110, -100, and -85 mV were calculated as the fraction of unblocked channels (F_{unb}) divided by the fraction of blocked channels ($1 - F_{unb}$). The fraction of unblocked channels was the same as the proportion of I_f unblocked, and the fraction of blocked channels was the proportion of I_f blocked. The natural logarithms of $K_{1/2}$ values were plotted against membrane voltage, and were fitted with a linear function. According to the modified Woodhull equation (Woodhull, 1973) derived by Heginbotham and Kutluay, 2004, the effective valence value, $z\delta$, was obtained from the negative slope value of the linear relationship:

$$\ln K_{1/2} = \ln K_{1/2}\,(0\text{ mV}) - z\delta F V_m/RT$$

where F is Faraday's constant, V_m is the membrane potential, R is the gas constant, T is the absolute temperature, and $\ln K_{1/2}\,(0\text{ mV})$ is the voltage-independent binding constant at 0 mV.

Voltage-dependence of activation

Normalized tail current amplitudes were plotted as a function of test potential and values were fitted with the Boltzmann function:

$$f(V) = I_{max} / (1 + \exp((V_{1/2}-V)/k))$$

where V is the test voltage, k is the slope factor, and $V_{1/2}$ is the midpoint of activation. The Boltzmann function assumes that channels only undergo from closed to open transition, and does not account for any intermediate closed or open states that may exist. After obtaining

25

activation traces for control, a different cell was used to evaluate the effects of lidocaine to ensure that any difference in midpoint of activation was not due to current rundown. Unpaired student's t-test was used to determine whether $V_{1/2}$ and k values were significantly different between control and after lidocaine addition.

Concentration-response relationship

The proportion of I_f unblocked (y) was plotted against lidocaine concentration on a logarithmic scale to generate a concentration-response relationship. Data points were fitted by a nonlinear least-squares procedure using a modified version of the Hill equation assuming that lidocaine does not inhibit currents completely:

$$y = 1 - I_{Max.\ Inhibition} / (1 + (IC_{50}/[Lidocaine])^n)$$

where IC_{50} is the half maximal inhibitory concentration, n is the Hill coefficient, [Lidocaine] is the lidocaine concentration in the bath solution and $I_{Max.\ Inhibition}$ is the proportion of I_f blocked at maximal inhibition.

Determining rates of activation and deactivation

Time constants for activation were generated using a double exponential fitting procedure, and a single exponential fitting procedure was used to generate the time constant for deactivation. Paired student's t-test was used to analyze differences in time constants between control and a specific lidocaine concentration tested on the same cell. Multi-group differences caused by various lidocaine concentrations were not assessed because of the variability in time constants between control values in different cells. Activation currents were fitted by double exponential function, according to the following equation:

26

$$I(t) = A_f \exp(-t/\tau_{fast}) + A_s \exp(-t/\tau_{slow}) + C$$

where A_f and A_s are current amplitudes of fast and slow components of current activation, respectively, τ_{fast} and τ_{slow} are the time constants for fast and slow components of current activation, respectively, and C is the steady-state current amplitude.

Deactivation currents were fitted by a single exponential function, according to the following equation:

$$I(t) = A \exp(-t/\tau_{deact}) + C$$

where A is the current amplitude of current deactivation and τ_{deact} is the time constant of current deactivation.

The relative amplitude of fast component of current activation was calculated:

$$A_f / (A_f + A_s)$$

where A_f and A_s are current amplitudes of fast and slow components of current activation, respectively.

Chapter 3: Results

3.1 Introduction

Results in this chapter aim to address the specific aims presented in Chapter 1, and are described in the order in which the specific aims are presented. The first section reports that inhibition of I_f by lidocaine is fast, reversible, and weakly voltage-dependent. This observation is supported by representative time courses and traces for different potentials tested. A specific quantitative parameter is chosen to evaluate the half maximal inhibitory concentration (IC_{50}) of lidocaine on the HCN1 channel. The next section (3.2) looks at activation curves and analysis on channel activation and deactivation kinetics, which provide information as to whether or not lidocaine affects gating of the channel. The following section (3.3) examines the effects of the permanently charged derivative of lidocaine, QX-314, on the channel when applied extracellularly. Lastly, properties of three mutants with single amino acid substitution in the pore-lining S6 region of HCN1 are presented in section 3.4. All three mutants display kinetic properties that differ from the wild-type. The properties of one mutant and its effects by lidocaine are explored in detail. Initial experiments performed to optimize experimental conditions are described in the discussion chapter, with the corresponding figure attached in the Appendices.

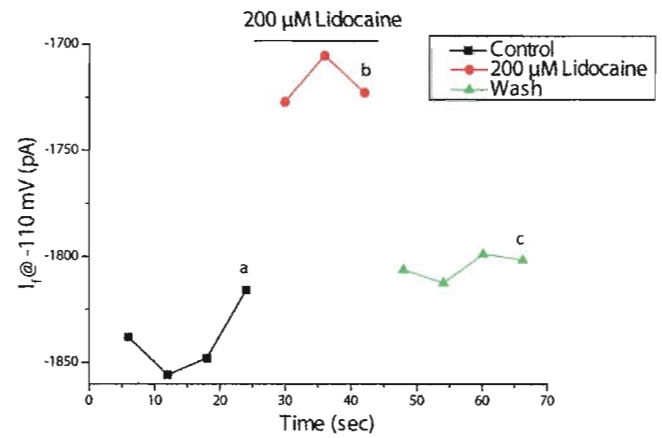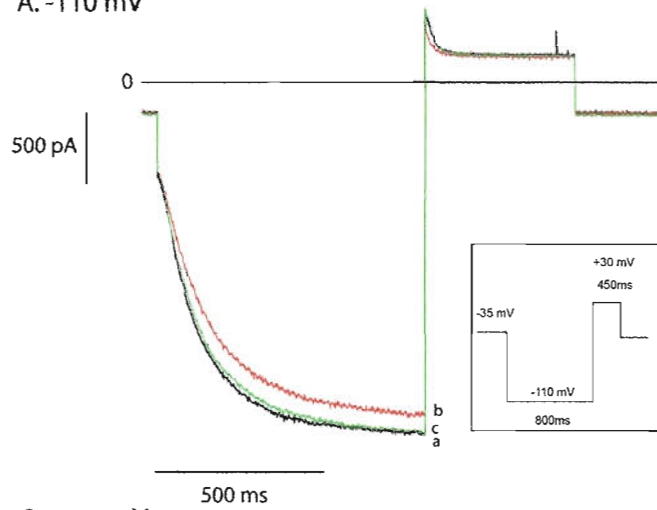## 3.2 Lidocaine inhibits the HCN1 channel in micromolar concentrations

HCN1 channel steady-state activation currents were examined in the presence of lidocaine in micromolar concentrations. Whole-cell currents were elicited by trains of activating/deactivating voltage steps applied every 6 seconds (Figure 3.1). This protocol was

28

applied at least 2-3 times prior to perfusion of 200 µM lidocaine. The current generated from the

activating step in each pulse was plotted over time. These current recordings prior to lidocaine

addition were denoted as control indicated by squares in the time course in Figure 3.1. Lidocaine

was then applied for approximately 3-4 sweeps or approximately 20 seconds until steady-state

inhibition was reached. The onset of lidocaine inhibition was fast, which was compatible with

lidocaine entry into the cell through the cell membrane in the uncharged form. Lidocaine

inhibition did not appear to be use-dependent, as inhibition did not accumulate with repeated

steps to open and close the channels. The control solution was re-introduced, and the protocol

was run for approximately 20-30 seconds to observe whether or not currents returned to the level

prior to lidocaine addition. The percent I_f reduction caused by 200 µM lidocaine was 6.6 ±

1.7 % (n = 3 cells), 8.3 ± 1.0 % (n = 7 cells), 17.1 ± 3.3 % (n = 7 cells) at -110 mV, -100 mV,

and -85 mV respectively (Figure 3.1), suggesting greater inhibition at less hyperpolarized

potentials. To assess the voltage-dependence in lidocaine inhibition, Woodhull analysis was

performed. A modified version of the Woodhull equation (Heginbotham and Kutluay, 2004)

was used in determining the delta (δ) value, which represents the percent penetration of lidocaine

into the transmembrane electric field. First, the fraction of unblocked channels (F_{unb}) was

calculated to be the fraction of I_f remaining, and the fraction of blocked channels ($1-F_{unb}$) was

derived from the fraction of I_f inhibited. The natural logarithm of the proportion of unblocked

channels versus blocked channels was then plotted versus the membrane potential, and the plot

was fitted with a linear function (Figure 3.2). The negative of the slope value yielded the z-delta

($z\delta$) value. Given that lidocaine can be either uncharged or possess a single positive charge, its

valence (z) value is +1 assuming that only the charged form participated in channel inhibition.

Figure 3.2 shows that lidocaine only sensed 4.5% of the transmembrane electric field from a δ

value of 0.045. Compared to a study that used a similar approach to assess voltage-dependence of inhibition (Heginbotham and MacKinnon, 1992), this z-delta value indicated weakly voltage-dependent inhibition by lidocaine on the HCN1 channel at hyperpolarized potentials.

Figure 3.1. Lidocaine, at 200 μM, inhibits HCN1 channels to a greater extent at less hyperpolarized potentials. Trains of activating/deactivating steps were applied every 6 seconds to Chinese hamster ovary (CHO) cells expressing HCN1 channels. (Left) Sample current traces were recorded just before lidocaine was added to the recording bath (a), at steady-state inhibition (b), and following washout (c). Voltage protocol is shown in the inset. (Right) Time course of HCN1 I_f currents recorded every 6 seconds. % I_f inhibition was determined by I_f reduction at steady-state inhibition relative to control, or the difference in I_f between (a) and (b) in the time course. % I_f reduction (mean ± SEM): 6.6 ± 1.7 % (n = 3) at -110 mV; 8.3 ± 1.0 % (n = 7) at -100 mV; 17.1 ± 3.3 % (n = 7) at -85 mV.

A. -110 mV

500 pA

500 ms

-35 mV
+30 mV
450ms
-110 mV
800ms

200 µM Lidocaine

Control
200 µM Lidocaine
Wash

I_f @ -110 mV (pA)

Time (sec)

B. -100 mV

500 pA

500 ms

-35 mV
-50 mV
2000ms
-100 mV
1000ms

200 µM Lidocaine

Control
200 µM Lidocaine
Wash

I_f @ -100 mV (pA)

Time (sec)

C. -85 mV

500 pA

500 ms

-35 mV
-50 mV
2000ms
-85 mV
1000ms

200 µM Lidocaine

Control
200 µM Lidocaine
Wash

I_f @ -85 mV (pA)

Time (sec)

32
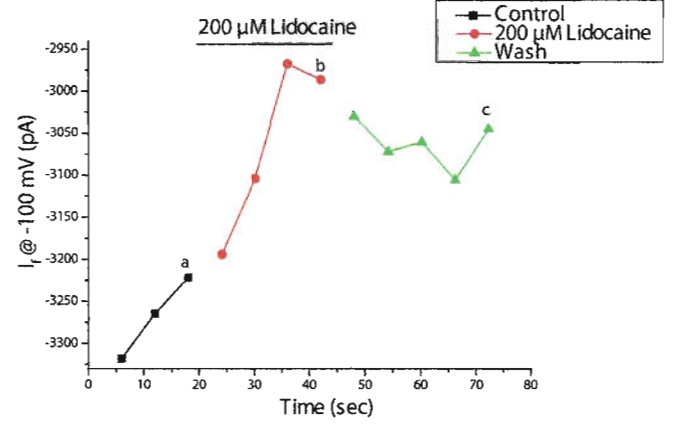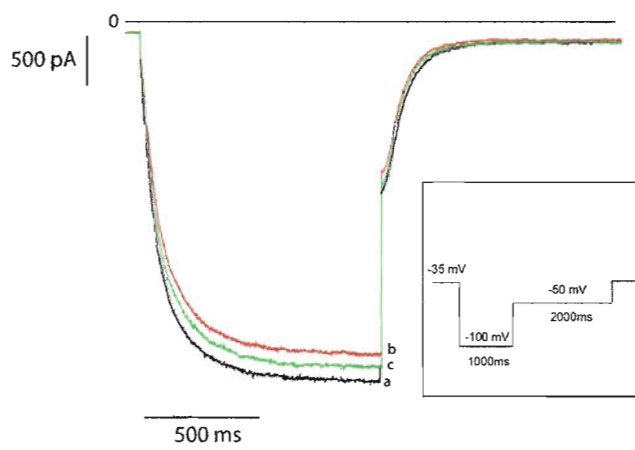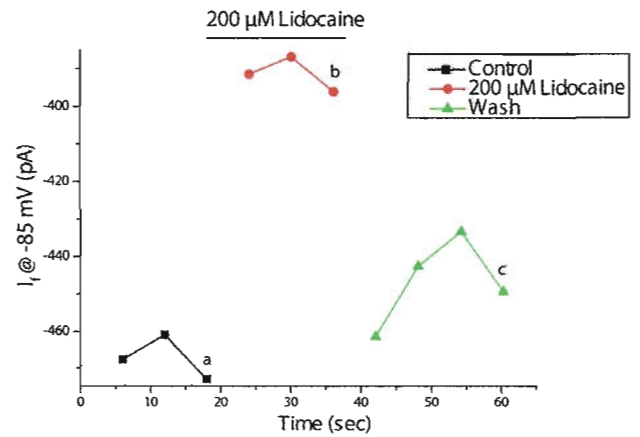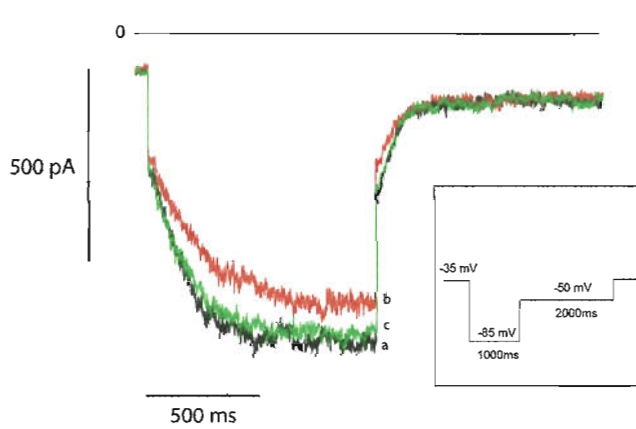
Figure 3.2. Linear fit of the modified Woodhull equation shows that lidocaine inhibition is weakly voltage-dependent. Natural logarithms of the binding constant ($K_{1/2}$) at -110, -100, and -85 mV were plotted against membrane potential, and fitted with a linear function. Error bars represent the SEM. The z-delta value ($z\delta$) derived from the negative slope value of the linear relationship suggests that lidocaine inhibition may be weakly voltage-dependent.
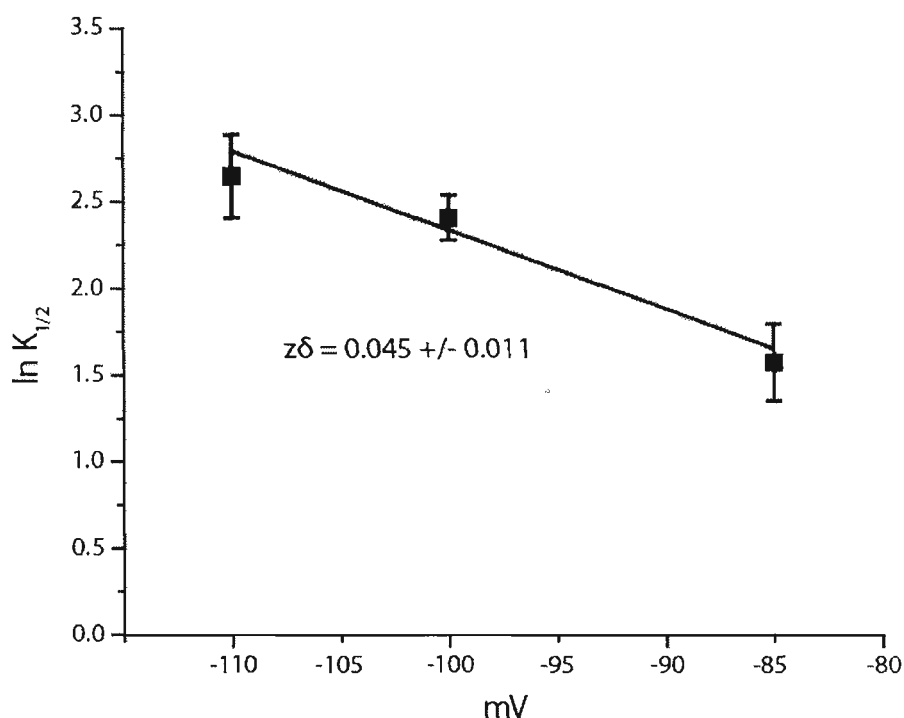
From current traces elicited by -110 mV for activation and +30 mV for deactivation, a greater proportion of current in the deactivation step appeared to be inhibited compared to the activation step. This current at +30 mV also appeared to be more stable during repeated activation/deactivation steps, and complete washout occurred in nearly every cell examined. Figure 3.3 shows representative current traces and time courses demonstrating the ability for current to return completely at +30 mV but not at all at -130 mV. The stability of the currents

and the reproducibility of these results at +30 mV led me to pursue experiments examining the effects of lidocaine at various micromolar concentrations. The percent I_f inhibition at +30 mV caused by 50, 100, 200, 400, 800, 1600, and 3200 µM lidocaine is shown in the concentration-response curve in Figure 3.3. The time for lidocaine inhibition to reach steady-state was fast (~6 seconds), and was dependent on concentration. To evaluate the half maximal inhibitory concentration (IC_{50}), the proportion of I_f unblocked was plotted versus lidocaine concentration on a logarithmic scale (Figure 3.3). The data points with the associated error bars were fitted with the Hill equation, yielding an IC_{50} value of 669 ± 320 µM (n = 3–7 cells), a Hill coefficient of 0.86 ± 0.15, and a maximum proportion of current inhibited of 0.88 ± 0.13 (mean ± SE). At the lowest lidocaine concentration tested of 50 µM, the percent I_f inhibited was 6.1 ± 2.0 % (mean ± SEM).

3.3   Lidocaine does not affect the voltage dependence of channel activation

It is possible that the observed lidocaine inhibition was due to a negative shift of the activation curve, leading to decreased number of channels activating at a specific potential. Thus, steady-state activation of HCN1 channels in the presence and absence of lidocaine was examined. I_f activation curves fitted with a Boltzmann function (Figure 3.4) revealed that the midpoint of activation ($V_{1/2}$) was -85.7 ± 1.7 mV (mean ± SEM; n = 6 cells) in the absence of lidocaine and -88.9 ± 1.2 mV (n = 6 cells) in the presence of 200 µM lidocaine. These values were not significantly different. There was also no significant difference in the slope factor (k), 13.3 ± 0.9 mV and 12.3 ± 1.0 mV (mean ± SEM) for control and with 200 µM lidocaine, respectively. At -110 mV, both activation curves (control and with 200 µM lidocaine) showed that approximately 90% of the maximum number of channels were activated. Because there was no

change in the voltage range in which the channels open, lidocaine appeared to have no effect on the steady-state activation of HCN1.

Figure 3.3. Lidocaine inhibition of I_f elicited by the +30 mV deactivation step is concentration-dependent. (A) Trains of activating/deactivating steps were applied every 6 seconds to CHO cells expressing HCN1 channels. Sample current traces were recorded just before lidocaine was added to the recording bath (a), at steady-state inhibition (b), and following washout (c). Voltage protocol is shown in the inset. (B) Current traces generated by the +30 mV step (enclosed in the red rectangle in panel A). (C) HCN1 I_f current recordings shown in the time course were elicited by the +30 mV deactivating step. % I_f inhibition between (a) and (b): 23.7 ± 4.5 % (mean $\pm$ SEM; n = 7 cells) at +30 mV.

(D) Proportion of unblocked I_f (I / I_o) plotted against lidocaine concentration fitted with the Hill equation. Data were obtained from % I_f inhibition at +30 mV deactivating step as described in the top panel. Error bars represent the SEM. The number of cells examined at each concentration is shown in parentheses. Values generated from a nonlinear least-squares fit include IC_{50} (the half maximal inhibitory concentration of lidocaine), n (Hill coefficient), and proportion of I_f blocked at maximal inhibition. All three values are reported as mean $\pm$ SE.

A.

500 pA

+30 mV
450 ms

−35 mV

−130 mV

1000 ms

c
b
a

500 ms

B.

100 pA

200 ms

C.

200 µM Lidocaine

I_t @ +30 mV (pA)

a

b

c

Control
200 µM Lidocaine
Wash

320

300

250

200

150

0   20   40   60   80   100   120

Time (sec)

D.

1.0

0.8

0.6

0.4

0.2

I / I_o

(5)

(5)

(7)

(3)

(3)

(4)

(3)

At +30 mV:
IC_{50} = 669 +/− 320 µM
n = 0.86 +/− 0.15
Max. inhibition = 0.88 +/− 0.13

100   1000   10000
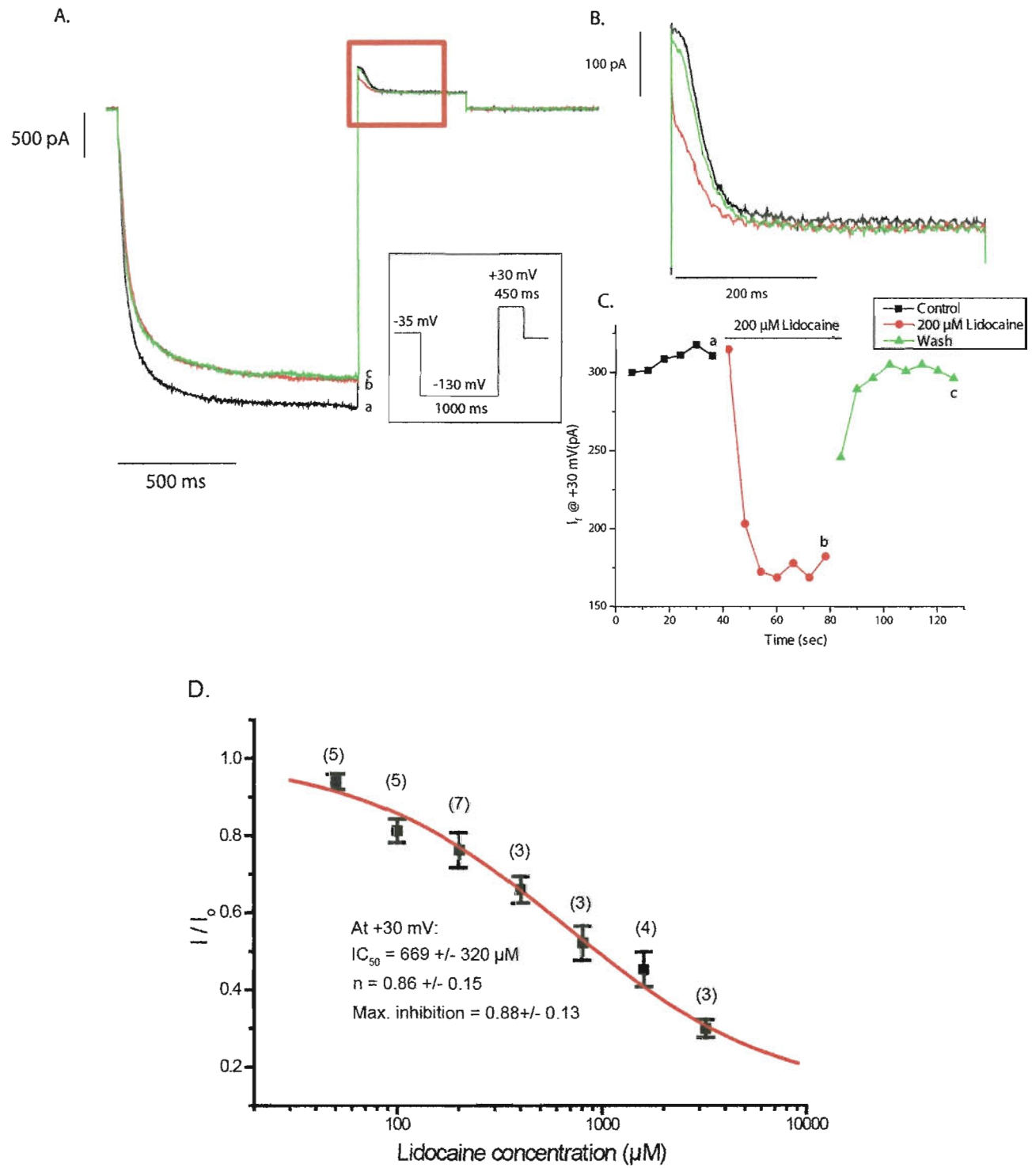
Lidocaine concentration (µM)

Figure 3.4. Lidocaine does not affect the voltage-dependence of HCN1 channel activation. (Top) Activation curves fitted with the Boltzmann function from 6 cells not treated with lidocaine and 6 cells treated with 200 μM lidocaine. Error bars represent the SEM. The midpoints of activation ($V_{1/2}$) for control and lidocaine were -85.7 ± 1.7 mV and -88.9 ± 1.2 mV (mean ± SEM), respectively. There was no significant difference between the midpoints of activation of control and 200 μM lidocaine. (Unpaired Student's t-test; p = 0.1444) The slope factor (k) was 13.3 ± 0.9 and 12.3 ± 1.0 mV (mean ± SEM) for control and lidocaine, which were not significantly different. (Unpaired Student's t-test; p = 0.4665) (Bottom) Representative current traces used to generate the activation curves.
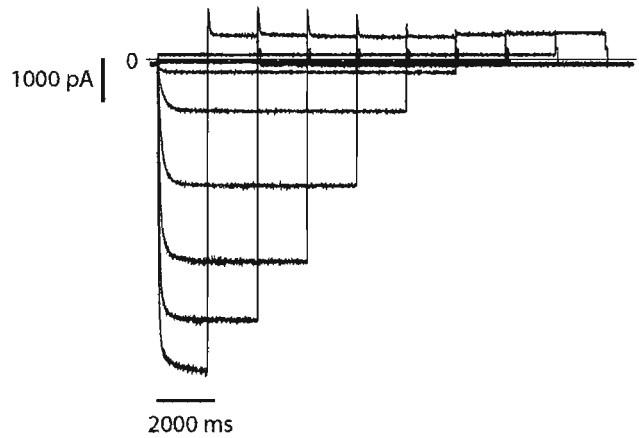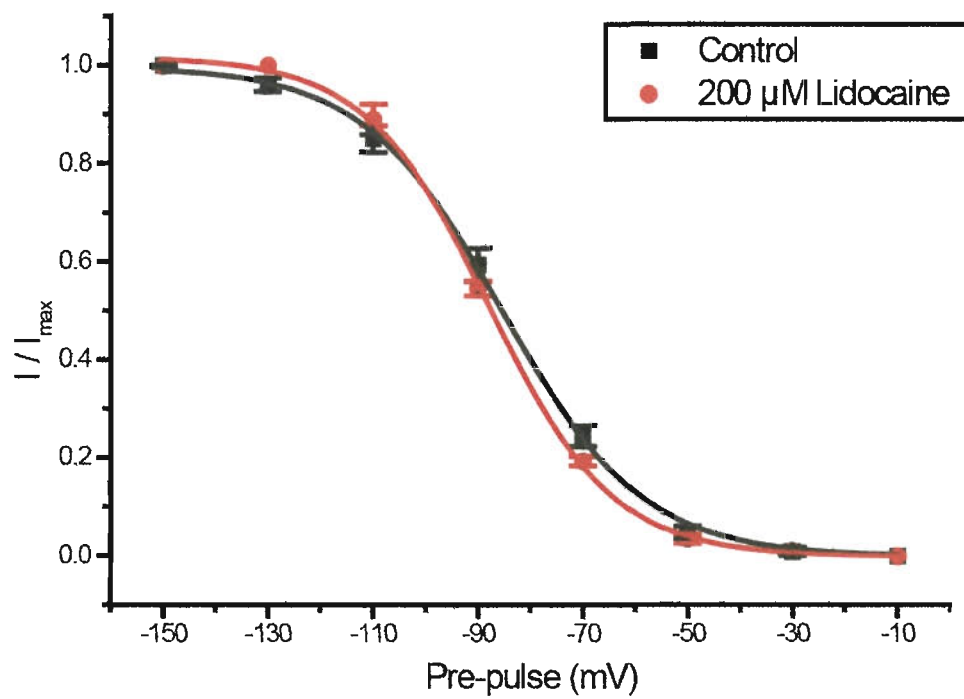
Control
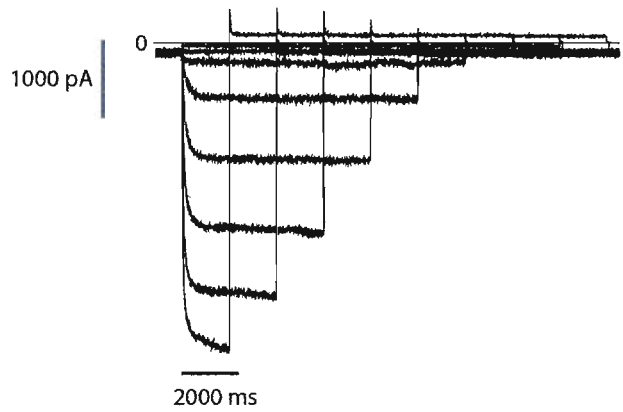
200 μM Lidocaine

3.4 Lidocaine does not affect the rates of activation and deactivation, but shortens the delay prior to deactivation

To examine how lidocaine affected the rates at which channels opened and closed, a double exponential function was used to describe activation currents and a single exponential function was used for deactivation currents. Figure 3.5 shows the double exponential function fitted curves for control and lidocaine activation currents. In both the control and lidocaine traces, an initial delay was observed prior to both activation and deactivation, which did not fit well with either a single or double exponential function and was excluded from the fitting procedure. A double exponential function fit described almost the entire activation process, whereas a single exponential function only fitted well with the initial ~200 ms of the activation process (data not shown). Comparison of the slow and fast components of the double exponential fits on activation (Figure 3.6) indicated that there was no significant difference in the activation kinetics after the addition of lidocaine ranging from 50 μM to 3200 μM, with the exception of the slow component at 400 μM. The percent of current amplitude that fitted with the fast component was 69.9 $\pm$ 2.2 % and 68.4 $\pm$ 2.3 % (mean $\pm$ SEM) for control and various lidocaine concentrations combined, respectively. The delay during deactivation in the control was considerably longer compared to activation. However, with lidocaine treatment, the delay prior to start of fitting deactivation currents was shortened, as can be appreciated in Figure 3.7. Figure 3.8 shows that the addition of lidocaine ranging from 50 to 3200 μM did not significantly affect the deactivation time constants. The delay prior to the start of fitting shown in Figure 3.8 was also important to indicate that the delay was significantly reduced at all concentrations with the exception of 200 μM. The discussion chapter addresses possible reasons for this delay and its significance in channel gating.

40

Figure 3.5. HCN1 activation currents are well described by a double exponential function. (Top) Activation current trace for control. (Bottom) Activation current trace in the presence of 200 μM lidocaine. The black trace is the raw trace, the red trace is the fitted curve, and the green trace represents the residuals of the fit (the difference between the raw trace and the fitted curve). With an initial delay, activation currents were fitted well with a double exponential function. A single exponential function could only describe the initial ~200 ms of the activation process (data not shown). The goodness of fit was determined by the residuals of the fit.
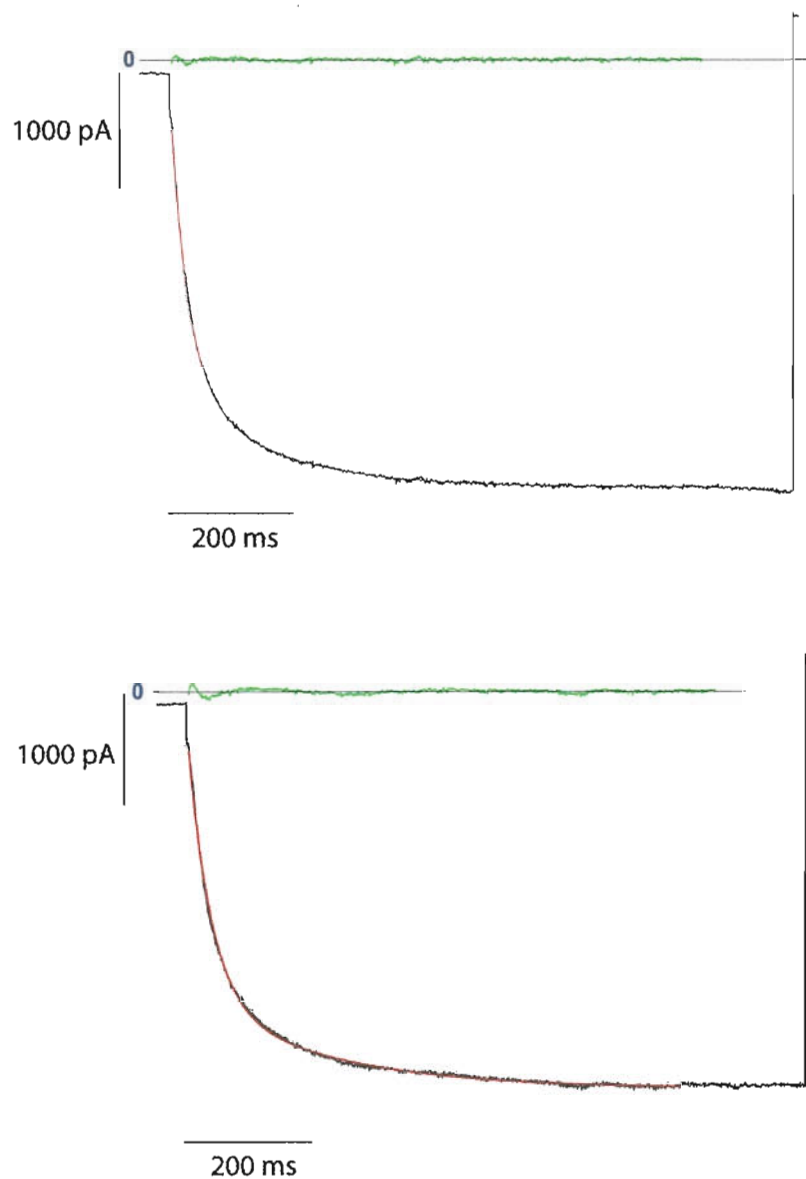
Figure 3.6. Lidocaine does not affect the rate of activation of HCN1 channels. Activation time constants were derived from double-exponential fits. Error bars and asterisks represent the SEM and $p < 0.05$, respectively. (Top) Comparison of the slow component of the fit between control and lidocaine treatment on the same cell showed no significant difference except at 400 μM. Student's paired t-test (two-tailed): 50 μM: $p = 0.4768$, n = 5; 100 μM: $p = 0.9846$, n = 5; 200 μM: $p = 0.7880$, n = 7; 400 μM: $p = 0.0290$, n = 3; 800 μM: $p = 0.2533$, n = 3; 1600 μM: $p = 0.1060$, n = 4; 3200 μM: $p = 0.3696$, n = 3.

(Bottom) Comparison of the fast component of the fit between control and lidocaine treatment on the same cell showed no significant difference at all concentrations. Student's paired t-test (two-tailed): 50 μM: $p = 0.5944$, n = 5; 100 μM: $p = 0.5665$, n = 5; 200 μM: $p = 0.1843$, n = 7; 400 μM: $p = 0.0832$, n = 3; 800 μM: $p = 0.2592$, n = 3; 1600 μM: $p = 0.0986$, n = 3; 3200 μM: $p = 0.0801$, n = 3.
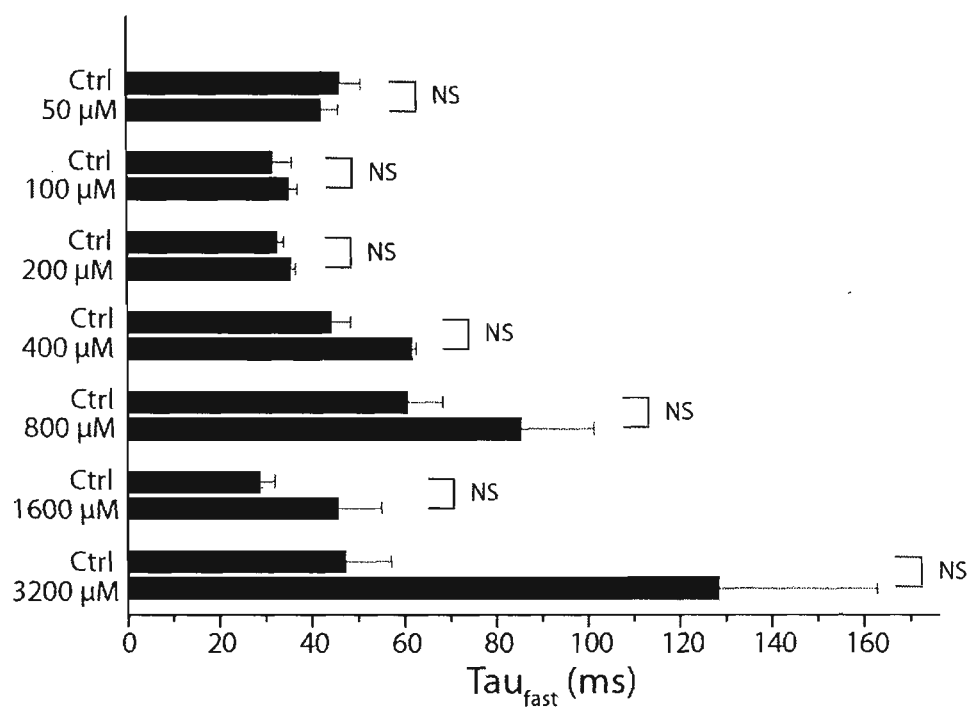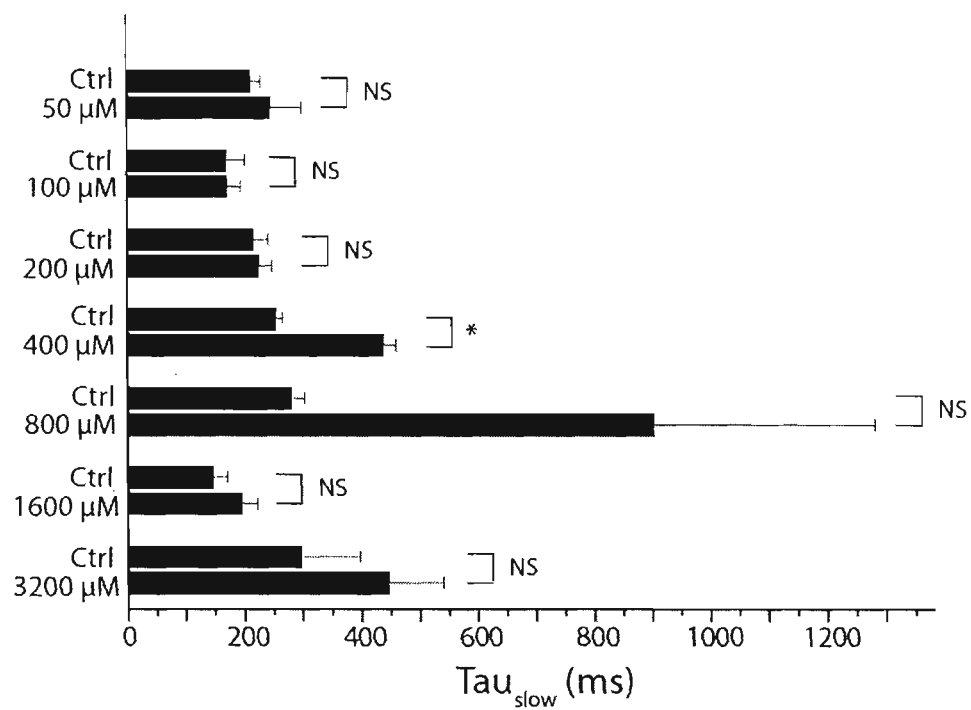
Figure 3.7. Lidocaine shortens the delay prior to the start of single exponential fit on deactivation currents. Representative current traces elicited by the +30 mV deactivation step for control (top) and following treatment with 3200 μM lidocaine (bottom). The black trace is the raw trace, the red trace is the fitted curve, and the green trace represents the residuals of the fit (the difference between the raw trace and the fitted curve). Fit of the respective traces with a single exponential function can only describe the deactivation currents well up to a certain point, as the initial 20 ms of the control and the initial 7 ms of the lidocaine trace cannot be described by a single exponential function. The difference in delay between control and lidocaine deactivation traces is quantified in Figure 3.8.

Delay prior to start fit = 20 ms

100 pA

0

100 ms

Delay prior to start fit = 7 ms

50 pA

0

100 ms

45
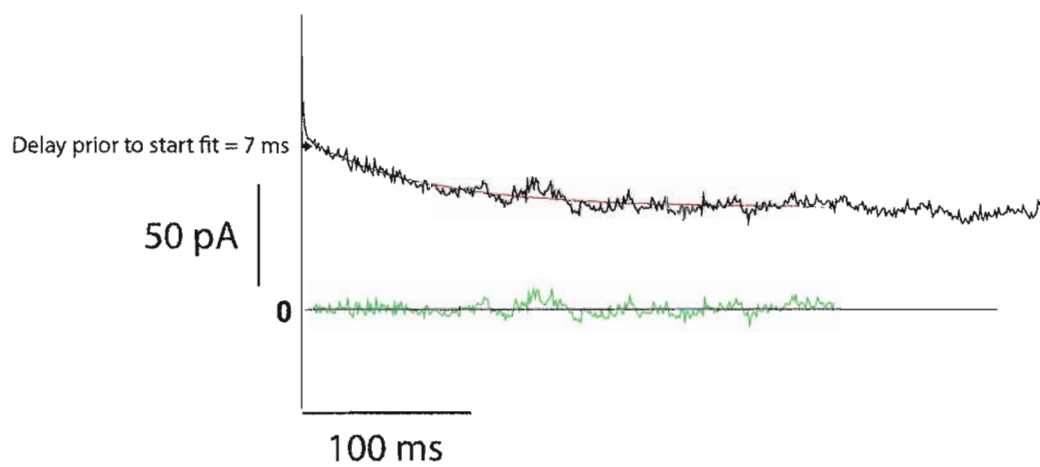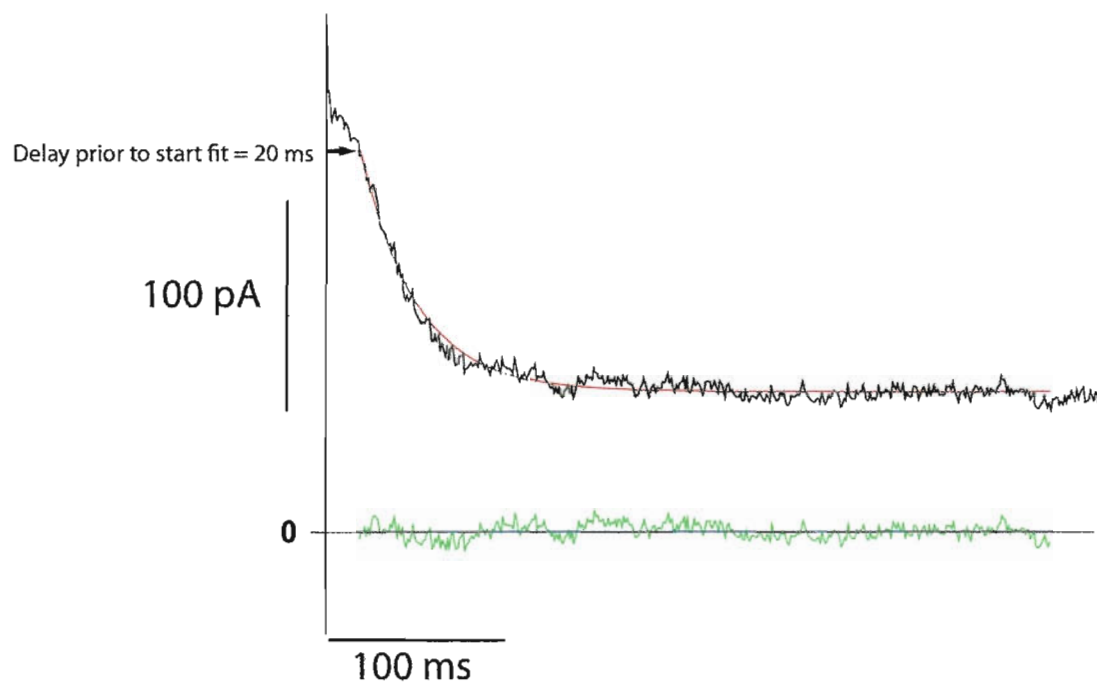
Figure 3.8. Lidocaine does not affect the rate of deactivation of HCN1 channels, but affects the delay prior to the start of a single exponential fit. Error bars and asterisks represent the SEM and $p < 0.05$, respectively. (Top) Deactivation time constants derived from single exponential fits. Comparisons were made between values from control and lidocaine treatment on the same cell. Student's paired t-test (two-tailed): 50 μM: $p = 0.0646$, n = 5; 100 μM: $p = 0.1158$, n = 5; 200 μM: $p = 0.5485$, n = 7; 400 μM: $p = 0.4468$, n = 3; 800 μM: $p = 0.8379$, n = 3; 1600 μM: $p = 0.6884$, n = 4; 3200 μM: $p = 0.2614$, n = 3.

(Bottom) Delay prior to the start of single exponential fit as described in Figure 3.7. The delay appeared to be removed upon addition of lidocaine at all concentrations with the exception of 200 μM. Student's paired t-test (one-tailed): 50 μM: $p = 0.0025$, n = 5; 100 μM: $p = 0.0201$, n = 5; 200 μM: $p = 0.0932$, n = 7; 400 μM: $p = 0.0023$, n = 3; 800 μM: $p = 0.0017$, n = 3; 1600 μM: $p = 0.0110$, n = 4; 3200 μM: $p = 0.0327$, n =3.
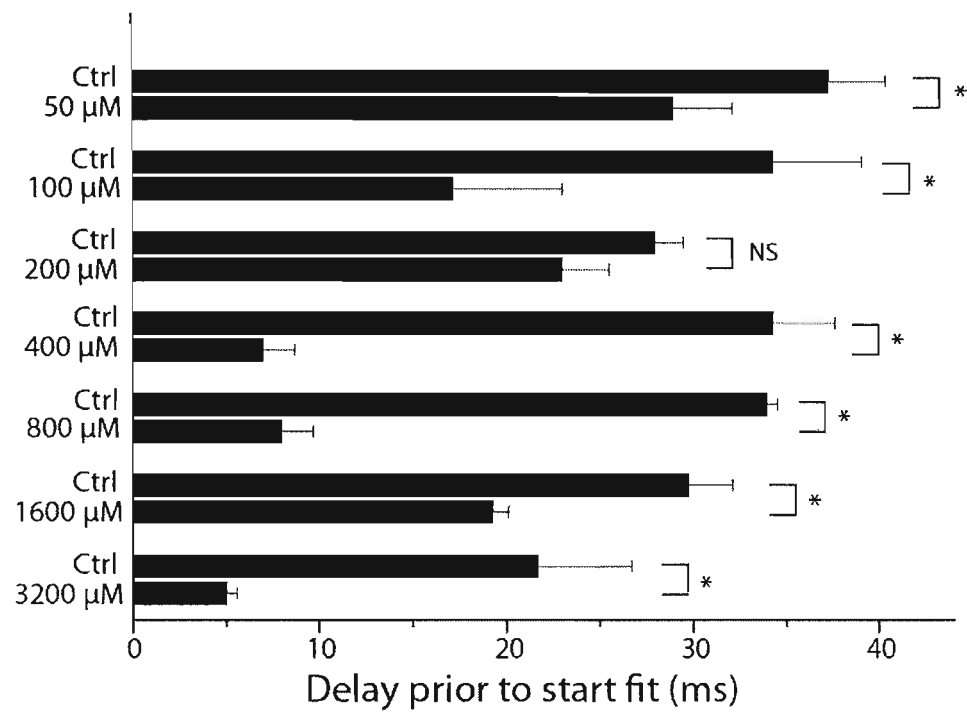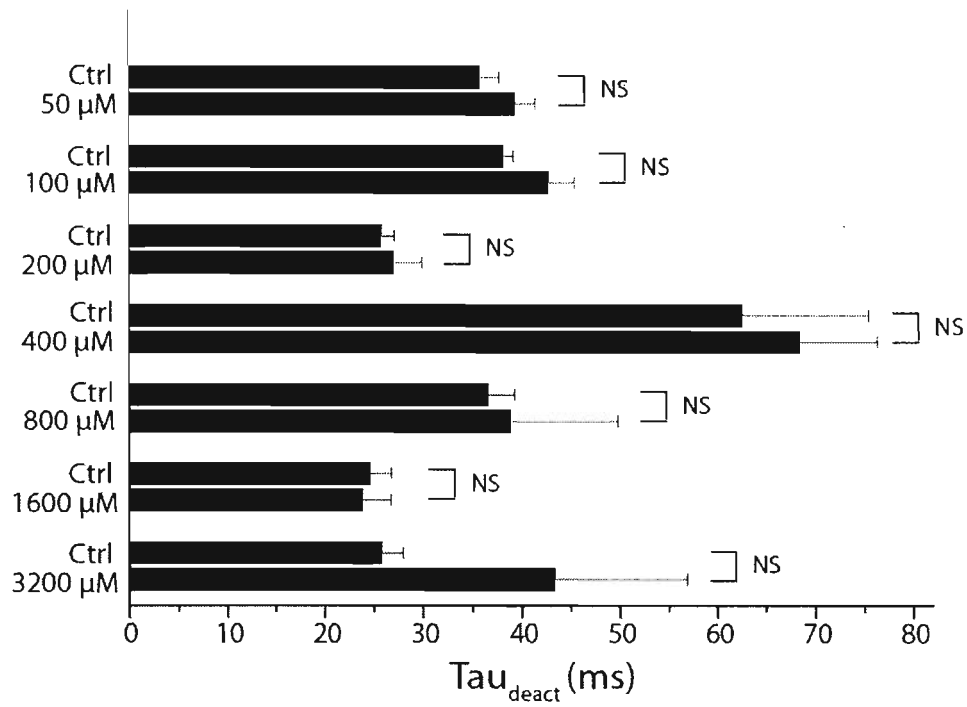
3.5   Extracellular application of the permanently charged derivative of lidocaine, QX-314, does not inhibit HCN1

To determine whether lidocaine inhibition, in its charged form, involved interaction with extracellular site(s), a protocol consisting of repeated activation/deactivation steps described above was performed with 500 µM QX-314 perfused into the recording chamber bath. The permanently charged derivative of lidocaine, QX-314, at a concentration of 500 µM, decreased I_f amplitude elicited by both the activation and deactivation steps (Figure 3.9). Currents recorded at +30 mV gradually reduced with each subsequent sweep following removal of QX-314, and did not show any current return. It is possible that this reduction in current was due to current rundown.

Figure 3.9. Extracellular application of 500 μM QX-314 reduces I_f elicited by the -110 mV activation step and the +30 mV deactivation step, without current recovery. Trains of activating/deactivating steps were applied every 6 seconds. I_f reduction was observed, but could not be distinguished from current rundown. (A) Sample current traces were recorded just before QX-314 was added to the recording bath (a), at steady-state inhibition (b), and following washout (c). Voltage protocol is shown in the inset. (B) Current traces generated by the +30 mV step (enclosed in the red rectangle in panel A) (C) Chemical structure of QX-314. (D) Time course showing HCN1 I_f currents elicited by the +30 mV deactivating step.
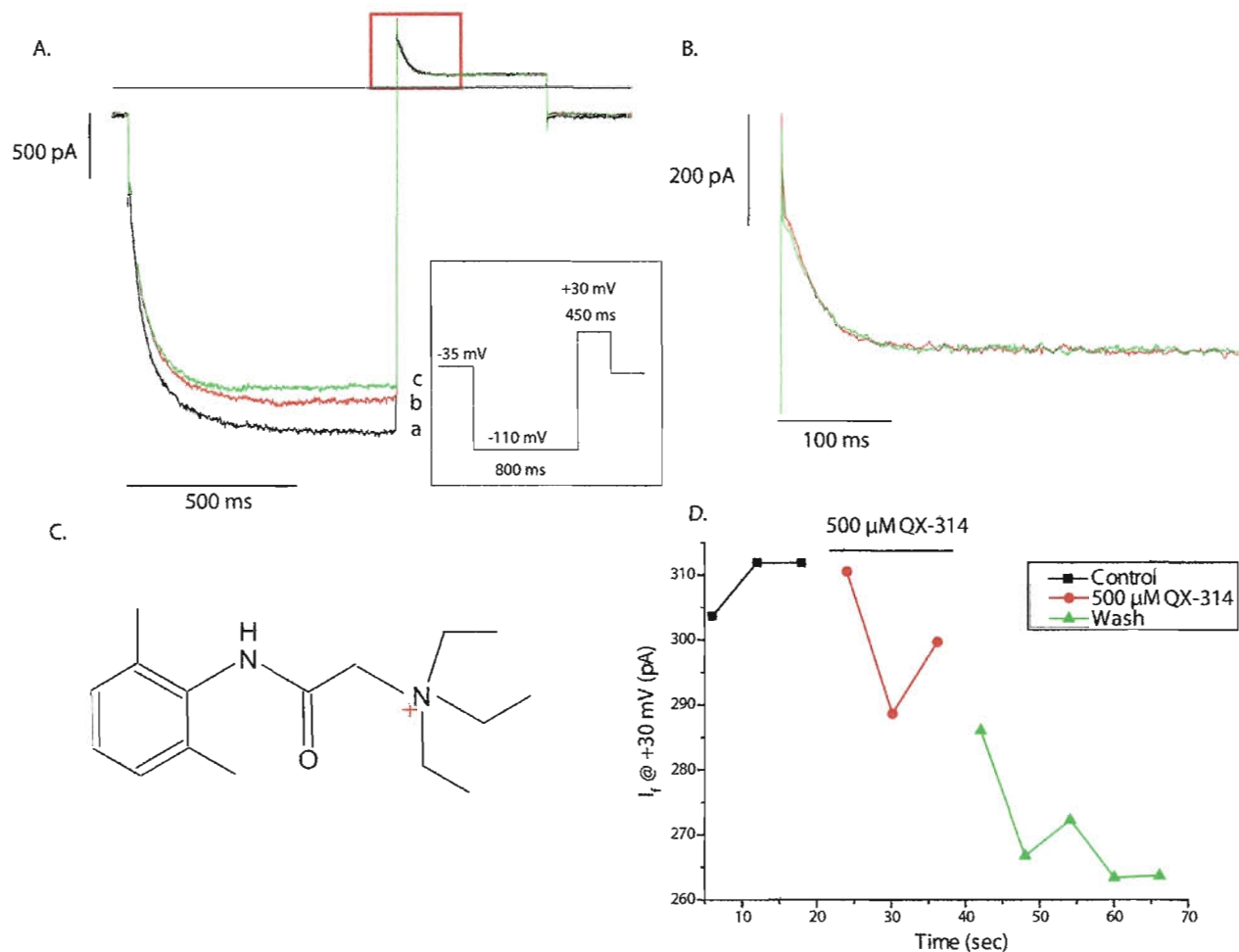
3.6 Properties of HCN1 mutants with single amino acid residue substitution

Three HCN1 mutants were made each with a single amino acid residue substituted in the pore-lining S6 region of the channel to determine whether lidocaine inhibition involved interaction with these residues. The A372G and V379A mutants were made to test whether the aromatic group of lidocaine interacts with the suspected hydrophobic cavity formed by the side chains of these amino acid residues (Cheng et al., 2007). The F378A mutant was produced to examine whether lidocaine, in its charged form, interacts with π electrons from the aromatic ring in phenylalanine. All three mutants were functional, with currents recorded from activation and deactivation steps. F378A was chosen for detailed analysis with lidocaine, as it provided relatively stable recordings compared to A372G and V379A. Representative current recordings of A372G and V379A can be found in the Appendix (Figures A2.1 and A2.2). Steady-state activation and rates of activation and deactivation were compared between wild-type and HCN1 F378A. Steady-state activation of F378A (Figure 3.10) showed that the midpoint of activation was -80.2 ± 2.7 mV (mean $\pm$ SEM; n = 4 cells), which was not significantly different from that of wild-type (-85.7 ± 1.7 mV). However, the slope factor was 19.2 ± 1.1 mV, which was significantly different from the value obtained from wild-type (13.3 ± 0.9 mV). At -130 mV, approximately 90% of the maximum number of channels was activated. The rates of activation and deactivation were significantly different between wild-type and F378A (Figure 3.11). The rate of deactivation was significantly prolonged, as shown in representative traces from wild-type and F378A (Figure 3.12). Activation currents in F378A appeared to reach steady-state within 1000 to 1500 ms, but deactivation currents required a minimum of 2000 ms to reach steady-state compared to 100 to 200 ms in wild-type. It is also interesting to note that the delay observed during the deactivation process in wild-type channels did not appear in F378A.

50

Figure 3.10. HCN1 F378A has a midpoint of activation ($V_{1/2}$) similar to that for the wild-type channel, but has a significantly different slope factor (k) . (Top) Activation curve fitted with the Boltzmann function from 4 cells expressing HCN1 F378A. (Bottom) Representative current traces used to generate the activation curve.

$$V_{1/2} = -80.2 +/- 2.7 \text{ mV}$$
$$k = 19.2 +/- 1.1 \text{ mV}$$

I / I_max

Pre-pulse (mV)

1000 pA

2000 ms
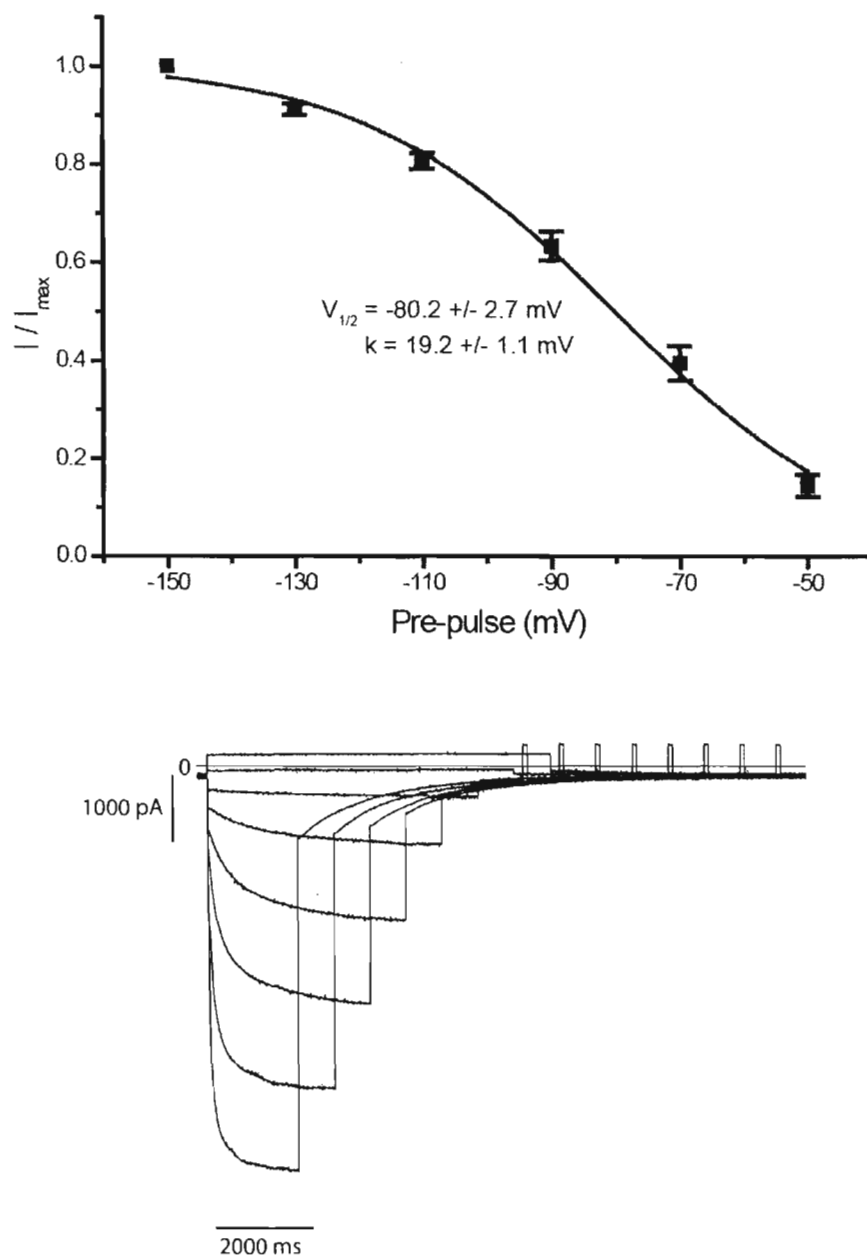
Figure 3.11. Activation and deactivation time constants are significantly different between wild-type HCN1 and HCN1 F378A. Error bars and asterisks represent the SEM and $p < 0.0001$ (unpaired Student's t-test), respectively. (A, B) Comparison of slow and fast components of double exponential fit on activation between wild-type and F378A. (C) Comparison of deactivation time constants between wild-type and F378A. Number of cells is indicated in parentheses.
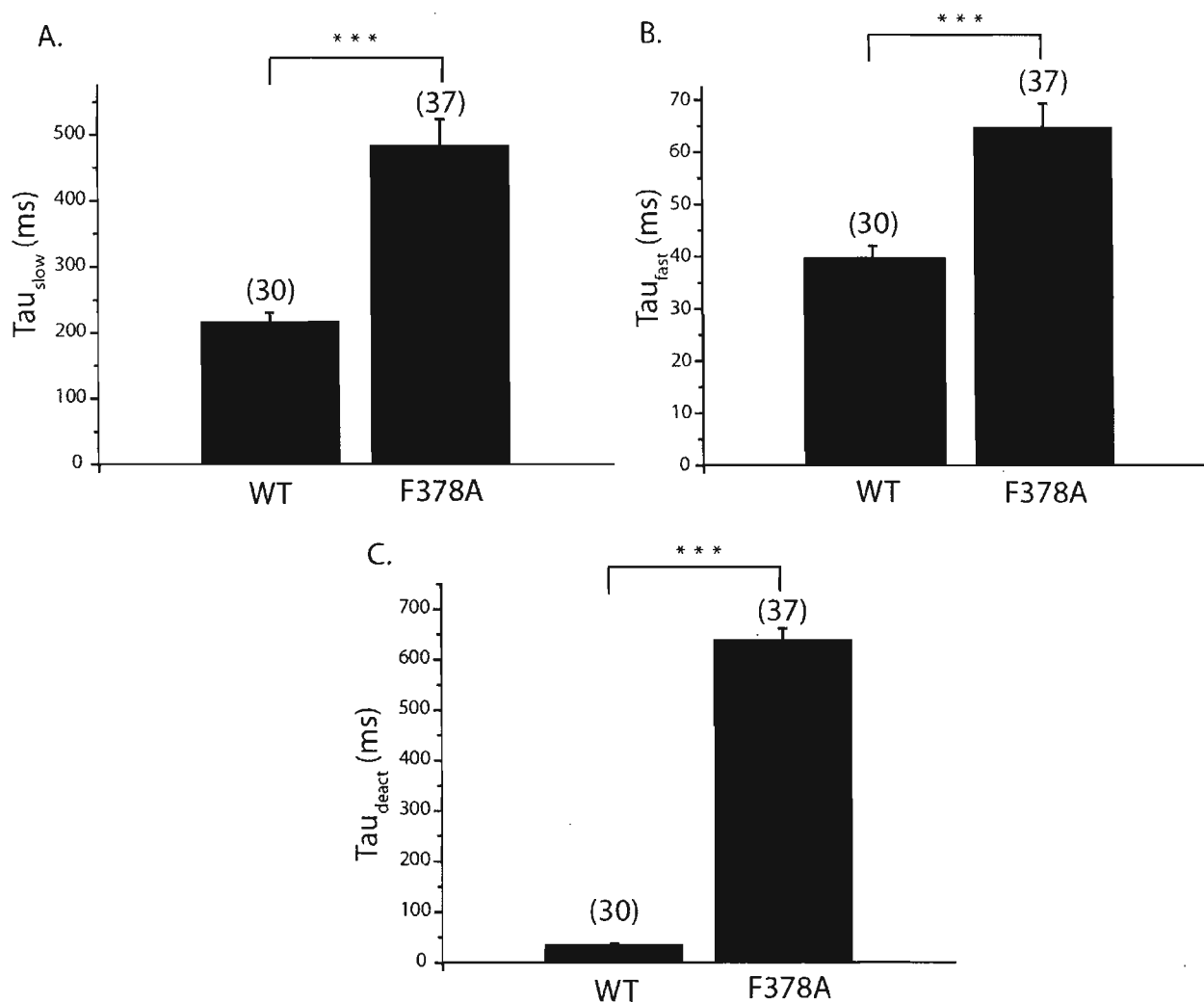
Figure 3.12. HCN1 F378A deactivates more slowly compared to wild-type. (Top) Deactivation currents elicited by +30 mV deactivation step reached steady-state within approximately 100 ms in wild-type. (Bottom) Deactivation currents elicited by +30 mV deactivation step did not reach steady-state within the same time scale as above. Full deactivation current trace is shown in the inset, with the portion enclosed in the red rectangle enlarged for comparison with wild-type. Note that the delay or "plateau" is present in wild-type but absent in F378A.
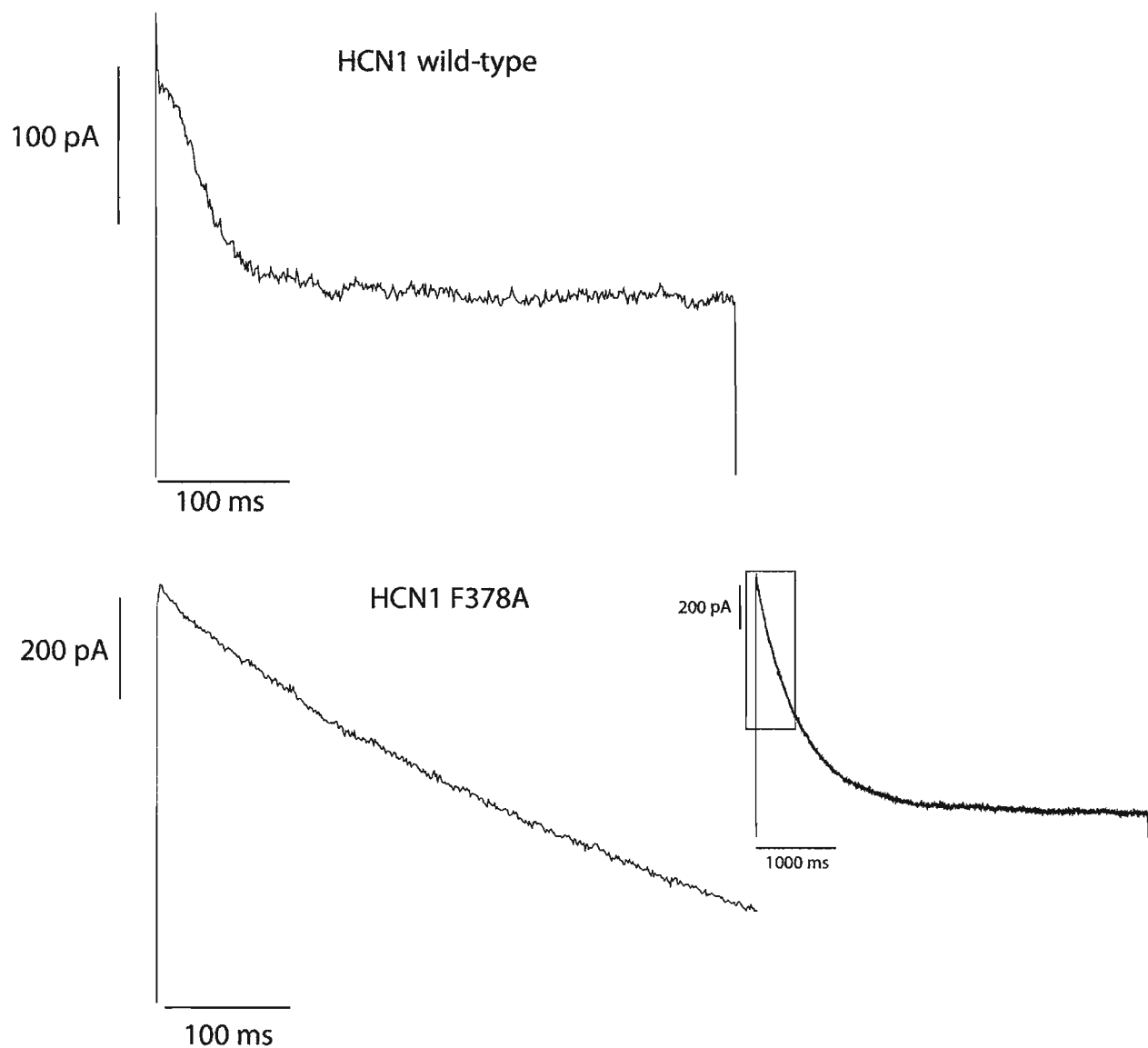
The proportion of I_f inhibited was then examined using -130 mV to activate the channel in trains of activation and deactivation steps repeated every 8 seconds. Similar to studies on the wild-type channel, recordings of I_f elicited by the +30 mV deactivation step were stable and the effect of lidocaine was reversible (Figure 3.13). The duration of the deactivation step was extended to 5000 ms to ensure that the steady-state was reached. Despite holding the cell at +30 mV for a prolonged period of time allowing up to 12 repeated pulses, currents in most cells were stable enough for I_f to be accurately calculated. Similar to the wild-type channel, I_f recorded at +30 mV was plotted over time to show the effects of lidocaine and washout (Figure 3.13). Various lidocaine concentrations were tested on F378A, and the proportion of I_f inhibited increased with increasing lidocaine concentration (Figure 3.14). Compared to data for wild-type, a greater proportion of I_f was inhibited at lower concentrations tested (≤ 200 µM) in F378A. The data were not well described by the Hill equation, and were not presented in a concentration-response curve. Data from the range of concentrations tested might have formed the steepest portion of the Hill plot without the top and bottom plateaus. There was a significant difference in the rates of activation by 800 µM lidocaine for both the slow and fast components of the double exponential function fit, with 400 µM lidocaine also affecting the fast component (Figure 3.15). The deactivation time constant was significantly different with lidocaine application at concentrations ranging from 10 to 800 µM (Figure 3.16). It is important to note that both decrease in I_f amplitude and difference in deactivation time constant were attained with 10 µM and 20 µM lidocaine.

Figure 3.13. Lidocaine inhibition of I_f at +30 mV is fast and reversible in HCN1 F378A. Trains of activating/deactivating steps were applied every 8 seconds to CHO cells expressing HCN1 F378A. (A) Sample current traces were recorded just before lidocaine was added to the recording bath (a), at steady-state inhibition (b), and following washout (c). Voltage protocol is shown in the inset. (B) Current traces generated by the +30 mV deactivation step (enclosed in the red rectangle in panel A). (C) Time course of HCN1 I_f currents recorded every 8 seconds. % I_f inhibition between (a) and (b) (mean ± SEM): 26.6 ± 1.4 % (n = 4) at +30 mV by 200 μM lidocaine.

A.

2000 pA

0

2000 ms

-35 mV

+30 mV
5000ms

-130 mV

1500ms

b
a

B.

200 pA

1000 ms

C.

I_f @ +30 mV (pA)

Time (sec)

a

c

b

— Control
— 200 μM Lidocaine
— Wash
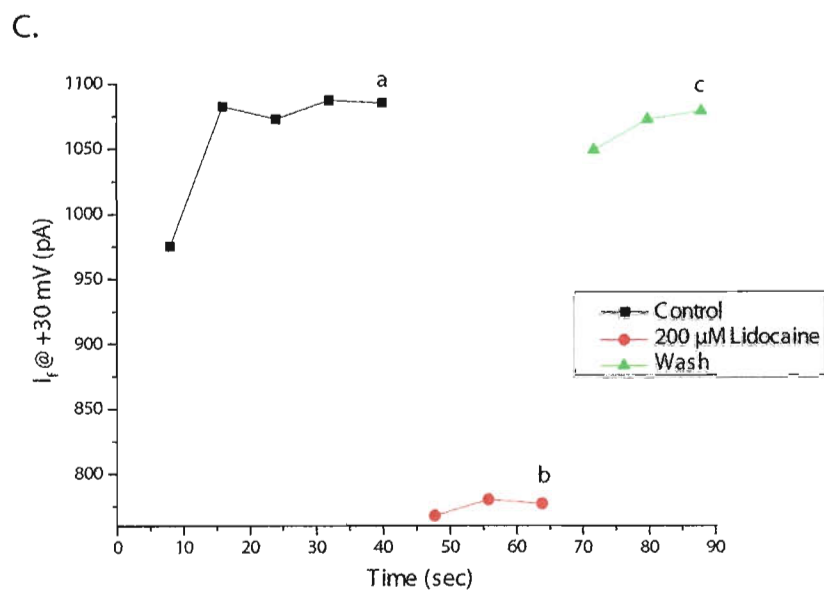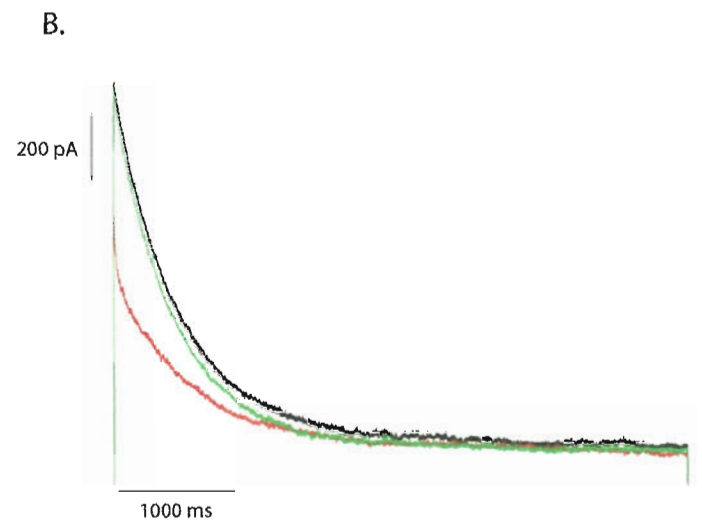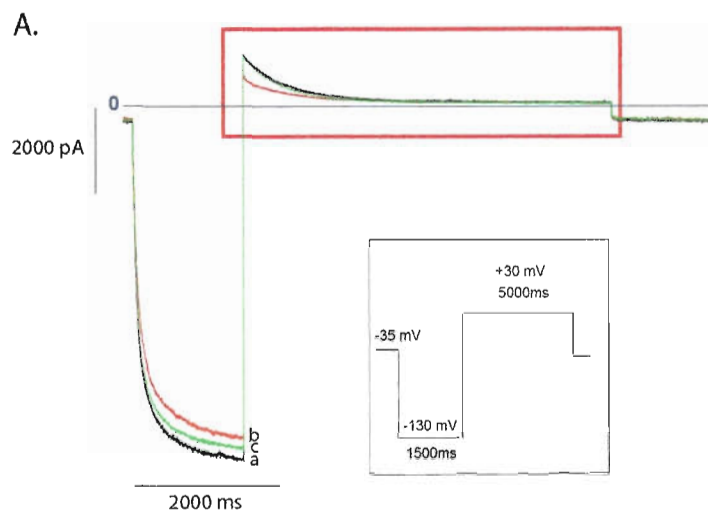
Figure 3.14. Lidocaine inhibition of I_f at +30 mV increases with lidocaine concentration in HCN1 F378A. Data reported as mean ± SEM (n = 4 – 8 cells). One-way ANOVA p < 0.0001. * p < 0.05. ** p < 0.01. *** p < 0.001.
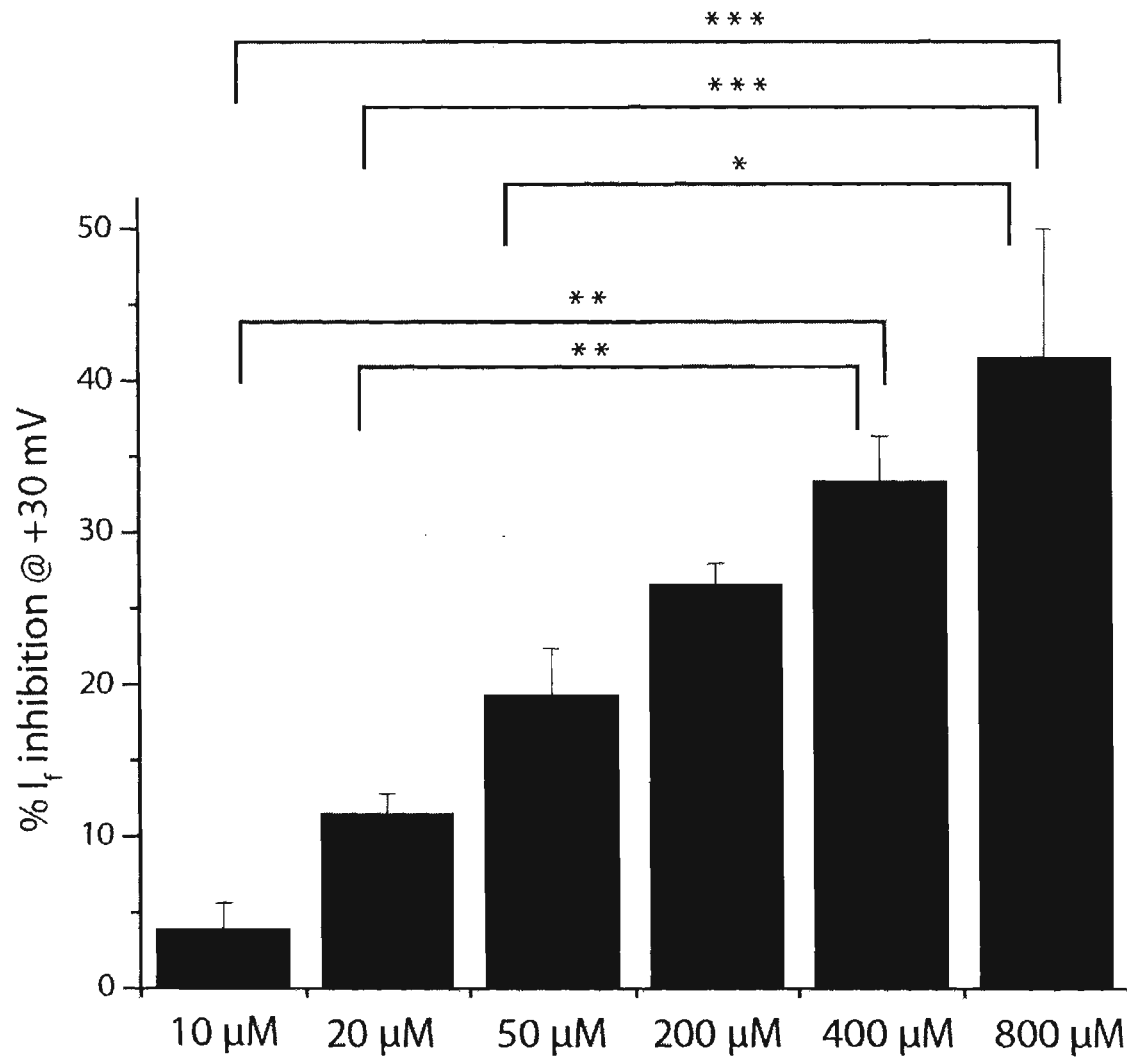
Figure 3.15. Lidocaine does not affect the rate of activation of HCN1 F378A at concentrations below 400 µM. Activation time constants were derived from double-exponential fits. Error bars and asterisks represent the SEM and $p < 0.05$, respectively. (Top) Comparison of the slow component of the fit between control and lidocaine treatment on the same cell showed no significant difference except at 800 µM. Student's paired t-test (two-tailed): 10 µM: $p = 0.0567$, $n = 4$; 20 µM: $p = 0.7530$, $n = 8$; 50 µM: $p = 0.1716$, $n = 6$; 200 µM: $p = 0.3640$, $n = 4$; 400 µM: $p = 0.1055$, $n = 8$; 800 µM: $p = 0.0022$, $n = 7$.

(Bottom) Comparison of the fast component of the fit between control and lidocaine treatment on the same cell showed no significant difference except at 400 µM and 800 µM. Student's paired t-test (two-tailed): 10 µM: $p = 0.0619$, $n = 4$; 20 µM: $p = 0.0520$, $n = 8$; 50 µM: $p = 0.5786$, $n = 6$; 200 µM: $p = 0.0514$, $n = 4$; 400 µM: $p = 0.0326$, $n = 8$; 800 µM: $p = 0.0021$, $n = 7$.
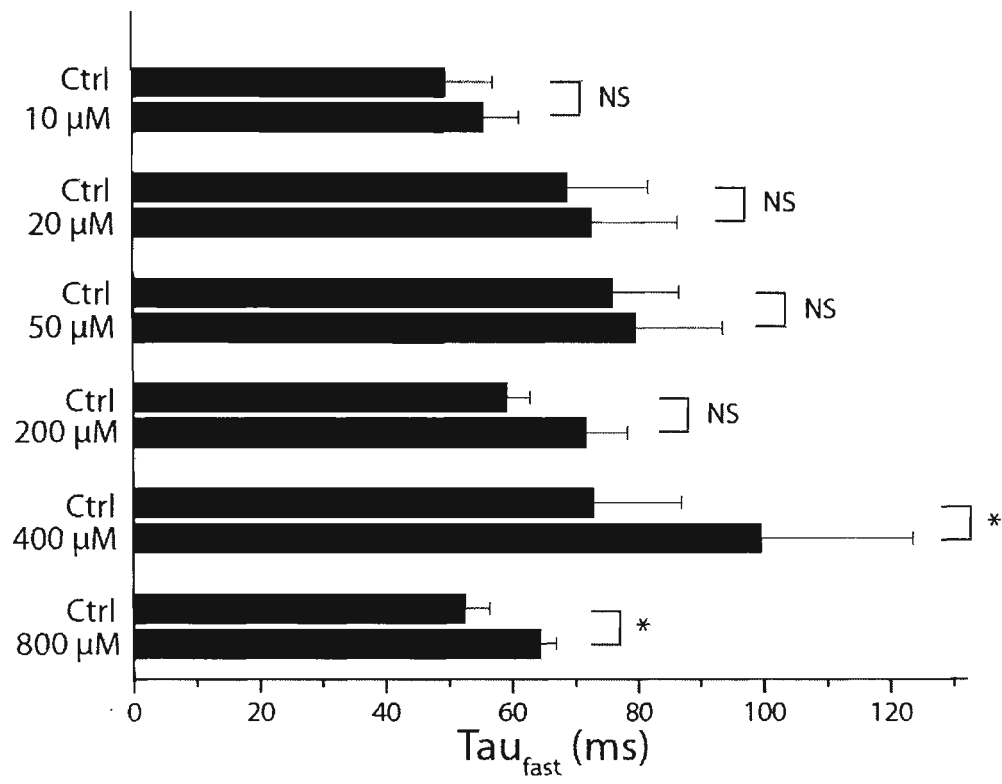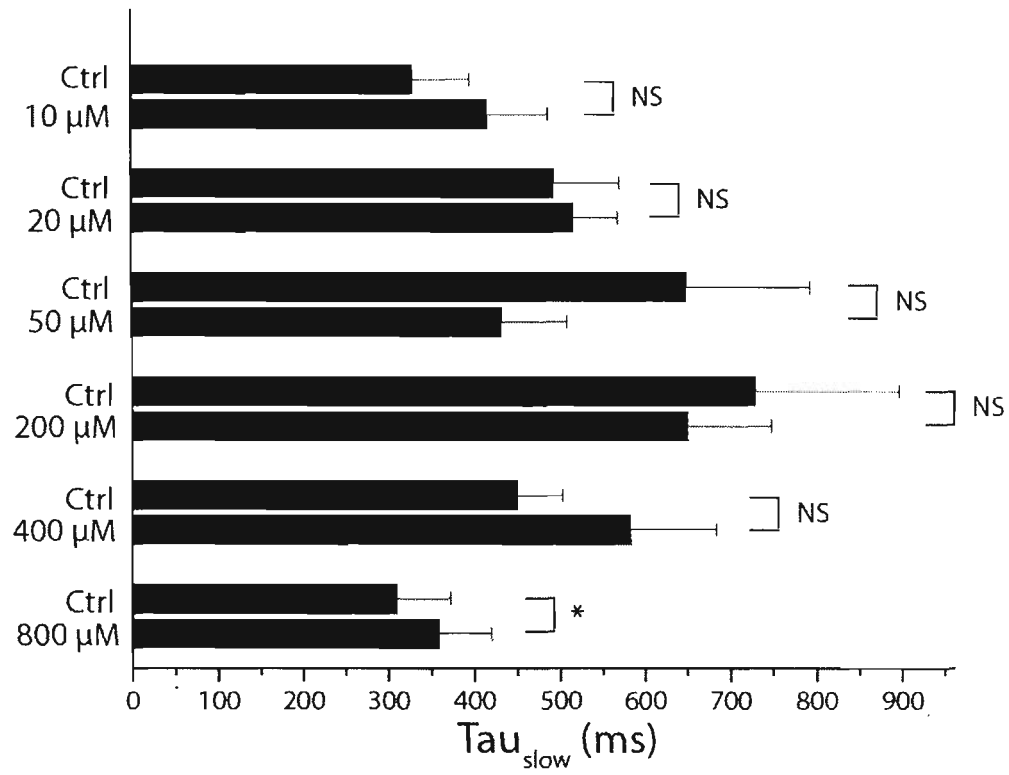
Figure 3.16. Lidocaine affects the rate of deactivation of HCN1 F378A. Deactivation time constants derived from single exponential fits. Comparisons were made between the respective control and lidocaine treatment on the same cell. Data reported as mean ± SEM. Student's paired t-test (two-tailed): 10 µM: p = 0.0202, n = 4; 20 µM: p = 0.0230, n = 8; 50 µM: p = 0.0495, n = 6; 200 µM: p = 0.0476, n = 4; 400 µM: p = 0.0427, n = 8; 800 µM: p = 0.0010, n = 7.
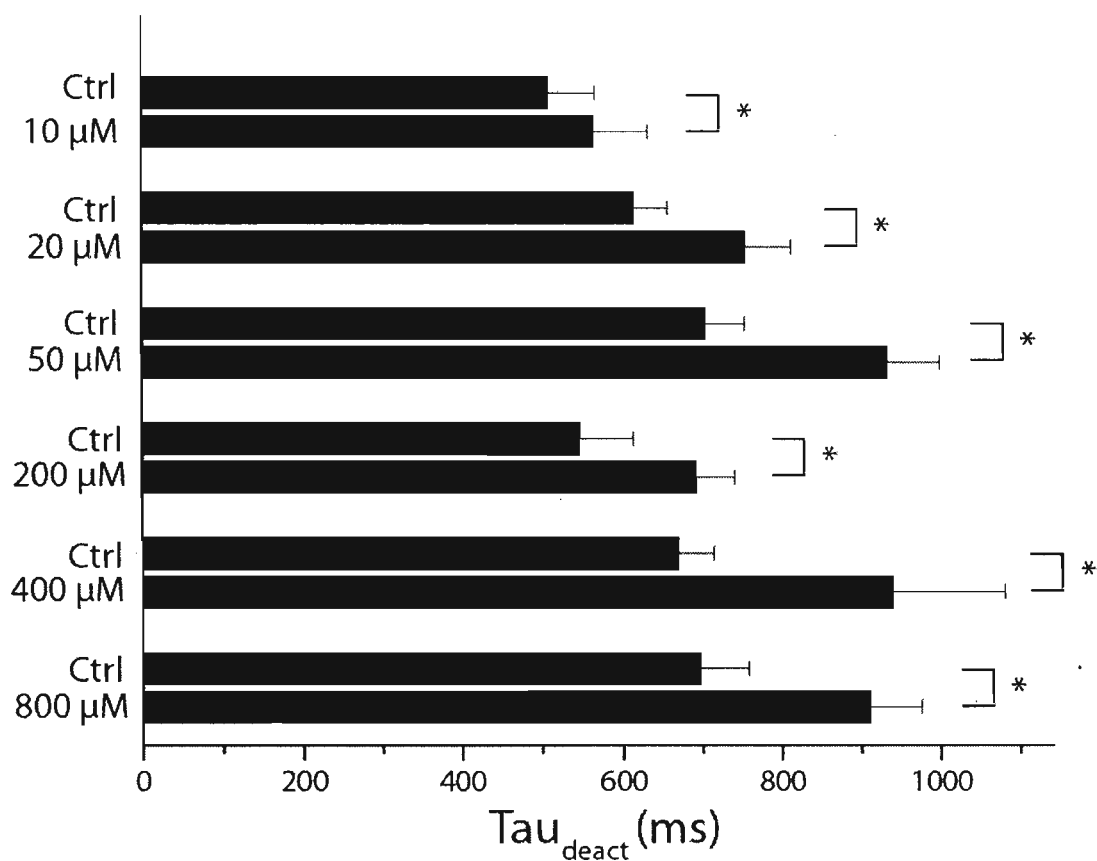
Chapter 4: Discussion

This chapter first provides a summary of my project, followed by a discussion of the findings in the previous chapter and work not presented, but used to optimize experimental conditions. Also, the significance of my project and future directions are discussed.

4.1   Summary of the study

The goal of my thesis is to determine whether lidocaine, in micromolar concentrations, inhibits the cloned HCN1 channel from the intracellular side. Specific aims were posed to examine various aspects of lidocaine inhibition. The first was to determine whether lidocaine inhibition was voltage-dependent and/or concentration-dependent. Increasing lidocaine concentrations exhibited greater percent of I_f inhibited at +30 mV, as represented by the concentration-response curve (Figure 3.3). Lidocaine inhibition appeared to be weakly voltage-dependent at hyperpolarized voltages in which more than half of the maximal number of channels is known to activate (Figure 3.2). The next objective sought whether activation and deactivation kinetics were altered in the presence of lidocaine. Parameters used for evaluation included voltage-dependence of activation and time constants of activation and deactivation. Activation curves comparing midpoints of activation and slope factors between control cells and cells treated with lidocaine revealed no significant difference in either value (Figure 3.4). The activation curves also showed that at least 90% of the maximal number of channels was activated at -110 mV (Figure 3.4). Activation currents were well described by a double exponential function compared to a single exponential function, whereas deactivation currents were fitted well by a single exponential function. Addition of lidocaine in concentrations used in the

concentration-response curve did not significantly affect the time constants for both activation and deactivation. A prolonged delay or "plateau" prior to the start of single exponential function fit of deactivation currents was observed, and was shortened or eliminated in current traces recorded with lidocaine present. Extracellular application of the permanently charged derivative of lidocaine, QX-314, at a concentration of 500 μM, decreased I_f amplitude, but could not be distinguished from current rundown (Figure 3.9). The last objective examined whether amino acid residues in the pore-lining S6 region were responsible for lidocaine interaction and inhibition. Three HCN1 mutants were generated, and were functional channels. F378A was selected for further analysis, as it provided relatively stable recordings during repeated activation/deactivation steps compared to A372G and V379A. Increasing lidocaine concentrations showed greater inhibition of I_f in F378A at +30 mV (Figure 3.14). Lidocaine, at concentrations ranging from 10 to 800 μM, increased the time constant of deactivation compared to control (Figure 3.16). The next section attempts to interpret findings described above, to address strengths and weaknesses with the study, and to relate findings in the literature.

4.2   Discussion of the findings

To test my hypothesis, I first performed experiments to examine whether lidocaine, at micromolar concentrations, inhibited currents from cloned HCN1 channels. Using trains of activation and deactivation steps, I_f elicited by the activation step was reduced upon addition of lidocaine. However, I_f started to decrease even before lidocaine was applied to the recording chamber, and steady-state inhibition could not be confidently determined. Also, in most cells, I_f continued to decrease after lidocaine was removed from the recording chamber, and showed no signs of current stabilizing or washout. The inability of currents returning to the control level

may be attributed to a phenomenon called current rundown, and/or the inability for lidocaine to washout completely.

Current rundown might have interfered with data interpretation and masked the effect of lidocaine. During prolonged dialysis in whole-cell recordings with HCN channels, rundown may occur (DiFrancesco et al., 1986; Pian et al., 2006). During current rundown, the voltage range in which the channels open may gradually shift to more hyperpolarized potentials and the maximum conductance at a certain potential may decrease over time. Rundown of I_f was also observed in single, dissociated sinoatrial node cells in whole-cell patch-clamp configuration (BoSmith et al., 1993). The exact mechanism for rundown is not known, but may be related to the loss of intracellular contents (Pian et al., 2006). Thus, once the cell membrane enclosed by the patch pipette is ruptured during a whole-cell recording, currents start to decrease over time. In our study, we only chose cells that yielded partial or complete return in current amplitude following the removal of lidocaine, which would not occur if the initial decrease was due only to current rundown.

Initial experiments were performed with lidocaine perfusion from the side of the recording chamber, and not directly on the cell under study. The intracellular solution in the patch pipette did not include 2 mM creatine phosphate, 2 mM Mg-ATP, 1 mM cAMP, and 20 μM PIP$_2$. Figure A1.1 in the Appendix shows representative current traces and time course from these initial experiments. Inhibition of lidocaine could not be distinguished from the linear decay in current shown in the time course. Also, each experiment required approximately 2.5 minutes and as many as 13 sweeps of activation and deactivation steps for steady-state inhibition to become apparent. Although current rundown may have attributed to the reduction in current amplitude, it was apparent that lidocaine inhibition took place, with the observation of current

return to the level prior to lidocaine addition. If current reduction was solely due to current rundown, currents recorded after lidocaine removal from the recording chamber would not have returned partially or completely to the level prior to lidocaine addition. Possible solutions to ensure accurate quantification of lidocaine inhibition included performing perforated patch-clamp experiments, altering the constituents of the intracellular solution in the patch pipette, and choosing only cells in which washout was complete or close to complete.

The latter two options were incorporated into the modifications to the experimental conditions, in order to minimize the effects of current rundown leading to stronger, more supportive data addressing the specific aims and hypothesis. In addition, a fast-step perfusion setup was installed to deliver lidocaine directly onto the cell under study. Using the fast-step perfusion setup, the cell was exposed to the desired concentration of lidocaine in approximately 20 ms, so that steady-state inhibition of lidocaine could be observed in less time. The duration for each experiment was shortened, which prevented prolonged dialysis of the cell and minimized the effects of current rundown. Constituents that are known to produce a depolarizing shift in channel activation, as described in the Materials and Methods section, were added to the intracellular solution in the patch pipette, which included creatine phosphate, Mg-ATP, cAMP, and PIP_2. Also, only cells in which currents returned at least 20 % to the level prior to lidocaine addition were used for analysis. These methodological adjustments vastly improved the quality of data, providing more accurate quantification of lidocaine inhibition.

Voltage-dependence of activation was examined to observe whether there was a shift in the midpoint of activation caused by lidocaine. To ensure that any shift in the midpoint of activation was due to lidocaine and not current rundown, one group of cells was designated as control and another was designated for lidocaine treatment. A lidocaine concentration of 200

μM was used, as initial experiments prior to the use of the fast-step perfusion setup showed the strongest evidence of lidocaine inhibition at this concentration. Figure 3.4 shows that there was no significant difference in either the midpoint of activation or the slope factor, which suggests that lidocaine did not affect the function of the voltage sensing regions (S1-S4) of the channel. Because there was no significant shift in the midpoint of activation, I_f reduction was most likely due to a decrease in maximal current amplitude. These results led to experiments testing I_f reduction at various hyperpolarizing potentials at which the channels open.

To test whether lidocaine inhibition was voltage-dependent, trains of activation and deactivation steps were applied in the presence of 200 μM lidocaine, with I_f determined from activation current traces elicited by -110 mV, -100 mV, and -85 mV. Steady-state inhibition was reached within one to three sweeps (6 to 18 seconds), which suggests that lidocaine bound to open channels very quickly and dissociated slowly from closed channels according to observations in Na^+ channels (Arthur and Strichartz, 1987). Even though lidocaine inhibition was clearly observed, current return was incomplete in most cells because of current rundown or incomplete washout. Also, I_f reduction was less than 20 % over the range of potentials tested. However, greater lidocaine inhibition at less hyperpolarized potentials may indicate that lidocaine, in its charged form, blocked from the inside of the channel. At less hyperpolarized potentials, lidocaine, with a positive charge, was more likely to be driven to the pore of the channel, as the intracellular environment was less negatively charged. Figure 3.2 shows a $z\delta$ value of 0.045. In a study examining the block of TEA^+ on potassium channels, the authors concluded that a $z\delta$ value of 0.04 was nearly voltage-independent (Heginbotham and MacKinnon, 1992).

Moreover, it also appeared from the current traces that there was greater I_f reduction at the +30 mV deactivation step. I_f recorded at +30 mV was more stable, which led to better reproducibility of results and more accurate quantification of lidocaine inhibition at lower concentrations. Complete washout also occurred in more cells. The concentration-response relationship in Figure 3.3 showed the half maximal inhibitory concentration to be approximately 669 µM. This value indicated that lidocaine had a weaker effect on HCN1 compared to cloned rabbit HCN4, I_h in rat small DRG neurons, and I_f in rabbit sinoatrial myocytes, which had reported IC_{50} of 276 µM, 99 µM, and 38 µM respectively (Bischoff et al., 2003; Rocchetti et al., 1999; Tamura et al., 2009). Differences in IC_{50} may be due to different isoform distribution from one tissue to another, different response to lidocaine between isoforms, different voltage protocols applied, and possible current rundown that was not accounted for in these studies.

Also, in studies on HCN4 and rabbit sinoatrial myocytes, experiments were conducted at 36°C, which may have altered the extent of lidocaine inhibition as well as the onset of lidocaine action possibly by modifying the pKa of lidocaine (Butterworth and Strichartz, 1990). Recordings in both studies were performed in Tyrode solution or low K^+ solution, in contrast to high K^+ extracellular solution used in this study. This difference in recording solution composition may explain the greater effect of lidocaine in these studies, as decreased current amplitude or inward ion flux may provide less resistance for lidocaine molecules to reach the binding site in the channel pore. Such dependence on current has been recently described for inhibition by ivabradine which is also thought to bind on the inner portion of HCN channels (Bucchi et al., 2002; Bucchi et al., 2006). Furthermore, the relatively low IC_{50} value obtained in the rabbit sinoatrial myocytes study may be due to native I_f channels consisting of different isoforms forming heteromers with or without accessory β-subunit(s). Comparing to results in

this study, it is likely that lidocaine has a greater affinity for heteromers or homomers consisting of other HCN isoforms. Other parameters generated from the concentration-response relationship include the Hill coefficient and the maximal proportion of I_f inhibited. The Hill coefficient was approximately one, which indicates that lidocaine has a single binding site or receptor. This is in accordance to the single receptor for local anesthetic binding in Na^+ channels (Hille, 1977a). The maximal proportion of I_f inhibited was also approximately one, but it remains unclear whether lidocaine can inhibit I_f completely. To improve data generated from the concentration-response relationship, in particular to reduce the standard error associated with the IC_{50} value, data can be collected at lower concentrations and at a high concentration where actual maximum inhibition is observed.

In wild-type HCN1, lidocaine did not affect the rates of channel activation and deactivation. The time constants of activation and deactivation for the control cells, however, varied considerably (Figures 3.6 and 3.8). For example, the activation time constant describing the fast and slow components of the double exponential function fit ranged from approximately 30 to 60 ms and 150 to 300 ms, respectively. The deactivation time constant ranged from approximately 25 to 60 ms. This variability could arise from cell-to-cell variability as well as errors in the fitting procedure. The standard errors of the mean were quite large in some test groups. This problem might have resulted in falsely determining that 400 µM lidocaine significantly affected the slow component of the activation time constant. However, the activation and deactivation time constants shown in figures 3.6 and 3.8 were comparable to previous studies describing the kinetics of HCN1 channels (Ishii et al., 2007; Moosmang et al., 2001; Santoro et al., 1998; Ulens and Tytgat, 2001). The fast component of the double exponential function fit on activation accounted for approximately 70 % of current amplitude,

which was in accordance with one of the initial studies characterizing HCN1 (Moosmang et al., 2001). From these findings, lidocaine appeared not to have disrupted the process of channel opening and closing, but affected the delay prior to the start of single exponential function fit of channel deactivation. Similar to the problem with determining activation and deactivation time constants, there was variability in the control data ranging from approximately 22 to 37 ms for the delay.

These findings provide information on how HCN1 channels activate and deactivate. A four-state allosteric model (Figure 4.1) has been described for HCN2 activation and deactivation kinetics involving voltage-dependent (C_R to C_A, O_A to O_R) and voltage-independent (C_A to O_A, O_R to C_R) transitions (Chen et al., 2007). Although this gating scheme appears to be quite simplified, it was shown to fit the opening and closing kinetics of HCN2 relatively well. In HCN2, both activation and deactivation could be fitted well with a single exponential function. Also, the delay or "plateau" was present upon steps to depolarized potentials, as it was more energetically favourable for deactivation to proceed through two sequential open states (O_A to O_R) to reach the closed state. A similar model can be used to describe HCN1 channel gating, with the exception that activation may require an additional closed state to represent the double exponential function used to fit activation currents. The deactivation process appeared to be similar to HCN2, as the delay or "plateau" was also observed in deactivation of HCN1. However, with the addition of lidocaine, it appears that the delay was reduced or, in some cases, abolished by lidocaine. The absence of this delay suggests that the channel did not undergo the transition from O_A to O_R. From these observations, lidocaine might have blocked the O_R state, preventing deactivation from proceeding through sequential open states. Assuming that the proposed model for HCN1 channel gating is accurate, channel deactivation would have to

undergo the reverse direction of activation. In response to the deactivation step, channels would proceed from the O_R state to an intermediate closed state, which might have resulted in the absence of the delay (Figure 3.7).

Figure 4.1. Four-state cyclic allosteric model for regulation of HCN2 opening and closing by voltage. C_R and C_A represent closed states with voltage sensors in resting and activated conformations, respectively. O_R and O_A represent open states with voltage sensors in resting and activated conformations, respectively. α and β represent voltage-dependent rate constants for activation and deactivation for the closed state, respectively. α' and β' represent voltage-dependent rate constants for activation and deactivation for the open state, respectively. *g* and *h* represent voltage-independent opening and closing rates respectively for the activated state. *g'* and *h'* represent voltage-independent opening and closing rates respectively for the resting state. (Chen et al., 2007), used with permission.
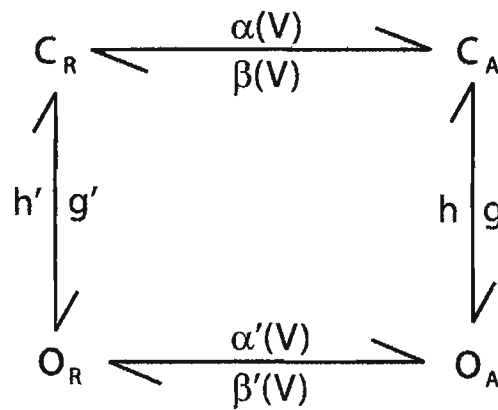
To determine whether lidocaine inhibition, in its charged form, involved extracellular site(s), the permanently charged derivative of lidocaine, QX-314, was applied extracellularly at a concentration of 500 μM. An immediate reduction in I_f was observed with the addition of QX-314 in panel D in Figure 3.9, but this current reduction could not be determined to be inhibition by QX-314 without any clear indications of current return. Currents did not return either because QX-314 did not washout, or that the observed effect was solely due to current rundown. Current rundown appeared to be greater at -110 mV than at +30 mV comparing panels A and B in Figure 3.9. However, when considering current reduction as a proportion of total current for both inward current at -110 mV and outward current at +30 mV, the proportion of current reduced due to current rundown in both cases are similar. In addition, current return probably should not be expected in the first place, as studies examining effects of intracellular QX-314 showed >90 % I_f inhibition at approximately 150 and 40 seconds after establishing whole-cell configuration without indications of current return (Kilb and Luhmann, 2000; Perkins and Wong, 1995). QX-314 was present in the bath solution for only three sweeps or approximately 20 seconds, to ensure consistency between this experiment and those with lidocaine. Further experiments using millimolar concentrations of QX-314 placed in the recording chamber bath for durations longer than 150 seconds might be needed to provide better indication as to whether or not extracellular QX-314 inhibits I_f.

Three mutants with single amino acid residue substitutions in the pore-lining S6 region were produced to determine whether lidocaine inhibition involved interaction with these residues. F378A was chosen for detailed analysis with lidocaine, as it provided relatively stable recordings during repeated activation/deactivation steps compared to A372G and V379A. Voltage dependence of activation in F378A was similar to wild-type, but activation and deactivation were

considerably slower (Figure 3.11). This difference in activation and deactivation kinetics may indicate that the side chain of phenylalanine could contribute to channel gating. Moreover, the delay prior to deactivation was not observed in F378A (Figure 3.12), suggesting that deactivation did not undergo the O_A to O_R transition in the proposed gating model. There was a similar trend in I_f reduction at +30 mV (Figure 3.14) compared to wild-type, with a greater proportion of I_f inhibited at concentrations less than 200 μM. If the phenylalanine residue were the sole determinant of lidocaine inhibition or interaction, substituting this residue with another residue without an aromatic ring in the side chain would theoretically remove lidocaine inhibition. With the proportion of I_f inhibited similar to wild-type at various micromolar concentrations and greater at lower concentrations, the phenylalanine residue is not responsible for lidocaine inhibition, and substitution to an alanine residue might have modified or enhanced lidocaine inhibition. Furthermore, with lidocaine inhibition observed in F378A, lidocaine could still inhibit the channel in the absence of the O_R state. Thus, the O_R state would not be responsible for lidocaine inhibition, contrary to speculations derived from wild-type data. Because lidocaine inhibition required channels in open state, lidocaine would most likely have greater affinity for the O_A state. This is supported by the fact that greater inhibition was observed at 20 μM lidocaine in F378A compared to 50 μM in wild-type. The increase in block at lower lidocaine concentrations in F378A compared to wild-type can be due to the O_A state being available for longer duration due to prolonged deactivation.

4.3   Significance

Results in this study suggest that the actions of lidocaine on I_f may be important for its effects as an antiarrhythmic drug and a local anesthetic. With the therapeutic concentration of

approximately 20 μM when administered intravenously as an antiarrhythmic drug (Burashnikov et al., 2007), it is obvious that lidocaine's antiarrhythmic effect does not require a concentration close to the IC_{50} value of 669 μM obtained in this study. Although the IC_{50} value is much higher than in the study examining inhibition of I_f in rabbit sinoatrial myocytes (38 μM) (Rocchetti et al., 1999), it is possible that a small percent I_f reduction, such as a 6.1% decrease in I_f with 50 μM lidocaine in this study, is sufficient to produce significant effects. However, the high IC_{50} value may indicate that the functional contribution to I_f by HCN1 may be less compared to other HCN isoforms such as HCN2 and HCN4. As a local anesthetic, lidocaine has been shown to block propagation of action potentials in peripheral nerves by inhibiting Na^+ channels (Butterworth and Strichartz, 1990). HCN1-mediated currents have been shown to be responsible for I_h in rat large and medium fast-conducting sensory neurons, and elimination of HCN1-mediated currents can lead to reduction in nociception (Momin et al., 2008). It is likely that lidocaine, at a concentration similar to the IC_{50} obtained in this study, can lead to reduction in nociception by inhibiting I_h. Lidocaine can potentially affect depolarization following the initial phase of afterhyperpolarization, leading to prolongation of the interval between action potentials in DRG neurons similar to observations on clonidine inhibition of I_h (Yagi and Sumino, 1998) (Figure 4.2). Although inhibiting I_h does not prevent generation of action potentials, slowing action potential propagation can be important physiologically in reducing pain.

Figure 4.2. Reduction in I_h can affect depolarization after the initial phase of afterhyperpolarization in action potentials in DRG neurons. Clonidine, an agent known to produce antinociceptive effects, inhibits I_h in rat DRG neurons and prolongs the interval between action potentials. (Modified from Yagi and Sumino, 1998, used with permission.)
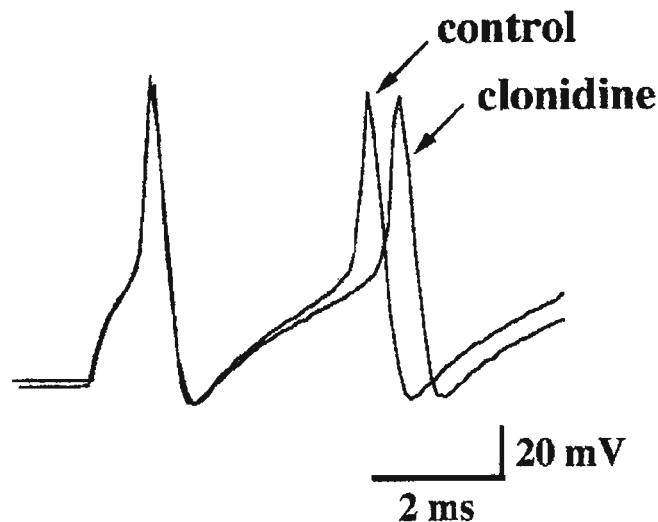
Comparison of lidocaine inhibition between Na^+ and HCN channels shows both similarities and differences. In our study, lidocaine inhibits I_f from HCN1 at +30 mV with IC_{50} of 669 µM, which is greater than 15 to 30 µM lidocaine used to produce significant inhibition on cardiac Na^+ channels (Bean et al., 1983; Grant et al., 1980; Hondeghem and Katzung, 1977) and 100 to 250 µM lidocaine used to inhibit Na^+ channels in nerves (Hille, 1977b). At a holding potential of -120 mV, approximately 10 % of Na^+ current is inhibited with 50 µM lidocaine (Bean et al., 1983), which corresponds to a similar reduction in I_f with 50 µM lidocaine. Based on findings in this study, it appears that lidocaine inhibition on HCN1, in its charged form, occurs from the intracellular side, which has been shown to be the mechanism in Na^+ channel inhibition. The phenylalanine residue in the pore-lining region is responsible for lidocaine

73

inhibition in Na^+ channels, but not in HCN1. The similarities in lidocaine inhibition between Na^+ and HCN channels suggest that the drug binding site could be located in the channel pore. The differences in inhibition between the two channels may be due to the fact that different gating mechanisms can greatly affect the mechanism and the rate by which lidocaine inhibits the channel. The speed of drug onset can be affected by the fact that HCN channels require more time to activate and do not undergo inactivation. Higher concentrations of local anesthetics are needed to block K^+ channels compared to Na^+ channels (Arthur and Strichartz, 1987). With HCN channels being more structurally similar to K^+ channels compared to Na^+ channels, higher concentrations of local anesthetics may also be needed to block HCN channels.

4.4 Directions of future study

This study has confirmed lidocaine inhibition on HCN1 channels, with molecular mechanism of inhibition yet to be determined. An alternate approach to examine whether π electrons of the phenylalanine at position 378 interact with lidocaine is to substitute the aromatic ring of phenylalanine at position 378 to a cyclohexane, thereby removing the π electrons without altering the side chain. To further elucidate the molecular mechanism by which lidocaine inhibited the channel, site-directed mutagenesis could be performed on other residues in the S6 region speculated to be involved in lidocaine inhibition. Tryptophan at position 362 and tyrosine at position 375 are possible candidates, as both amino acid residues possess an aromatic ring in which π electrons may participate in lidocaine interaction. Moreover, extracellular QX-314 experiments can be improved by placing QX-314 in the recording bath for a longer duration. To confirm whether lidocaine inhibition on I_f is from the intracellular side, QX-314 and lidocaine can be applied to inside-out patches. The reasons for the shortened delay in deactivation after

lidocaine addition, as well as the prolonged deactivation in F378A, are still unclear. Using results from this study, computations can be performed to construct an allosteric model for HCN1 channel gating.

To examine the relative functional contribution of each isoform to native I_f, protocols used in this study can be applied to examine the potencies of lidocaine on other cloned HCN isoforms such as HCN2 and HCN4, which are predominantly expressed in the heart as well as in rat small DRG neurons. Lidocaine has been shown to inhibit I_h in rat small DRG neurons, but effects on large DRG neurons have not been examined. Because HCN1-mediated currents have been shown to contribute to I_h in rat large and medium fast-conducting DRG neurons, lidocaine can be applied to rat large DRG neurons to confirm whether HCN1 currents is the sole determinant of I_h by comparing IC_{50} to this study. To test the effects of lidocaine at various membrane potentials, voltage protocols can be applied to simulate an action potential. This can determine inhibition by lidocaine on a specific isoform in physiological conditions. Lastly, inhibition of more potent amide-type local anesthetics such as bupivacaine and mepivacaine on HCN isoforms can be explored, ultimately determining whether these agents relieve pain in part by inhibiting I_h.

References

Accili, E.A., Proenza, C., Baruscotti, M., and DiFrancesco, D. (2002). From funny current to HCN channels: 20 years of excitation. News Physiol Sci *17*, 32-37.

Ahern, C.A., Eastwood, A.L., Dougherty, D.A., and Horn, R. (2008). Electrostatic contributions of aromatic residues in the local anesthetic receptor of voltage-gated sodium channels. Circulation Research *102*, 86-94.

Altomare, C., Bucchi, A., Camatini, E., Baruscotti, M., Viscomi, C., Moroni, A., and DiFrancesco, D. (2001). Integrated allosteric model of voltage gating of HCN channels. The Journal of General Physiology *117*, 519-532.

Arthur, G.R., and Strichartz, G.R. (1987). Local anesthetics (Berlin; New York, Springer-Verlag).

Barrow, A.J., and Wu, S.M. (2009). Low-conductance HCN1 ion channels augment the frequency response of rod and cone photoreceptors. J Neurosci *29*, 5841-5853.

Baruscotti, M., Bucchi, A., and Difrancesco, D. (2005). Physiology and pharmacology of the cardiac pacemaker ("funny") current. Pharmacology & Therapeutics *107*, 59-79.

Bean, B.P., Cohen, C.J., and Tsien, R.W. (1983). Lidocaine block of cardiac sodium channels. The Journal of General Physiology *81*, 613-642.

Biel, M., Schneider, A., and Wahl, C. (2002). Cardiac HCN channels: structure, function, and modulation. Trends in Cardiovascular Medicine *12*, 206-212.

Bischoff, U., Brau, M.E., Vogel, W., Hempelmann, G., and Olschewski, A. (2003). Local anaesthetics block hyperpolarization-activated inward current in rat small dorsal root ganglion neurones. British Journal of Pharmacology *139*, 1273-1280.

Bois, P., Bescond, J., Renaudon, B., and Lenfant, J. (1996). Mode of action of bradycardic agent, S 16257, on ionic currents of rabbit sinoatrial node cells. British Journal of Pharmacology *118*, 1051-1057.

BoSmith, R.E., Briggs, I., and Sturgess, N.C. (1993). Inhibitory actions of ZENECA ZD7288 on whole-cell hyperpolarization activated inward current (I_f) in guinea-pig dissociated sinoatrial node cells. British Journal of Pharmacology *110*, 343-349.

Bucchi, A., Baruscotti, M., and DiFrancesco, D. (2002). Current-dependent block of rabbit sino-atrial node I_f channels by ivabradine. The Journal of General Physiology *120*, 1-13.

Bucchi, A., Tognati, A., Milanesi, R., Baruscotti, M., and DiFrancesco, D. (2006). Properties of ivabradine-induced block of HCN1 and HCN4 pacemaker channels. The Journal of Physiology *572*, 335-346.

Burashnikov, A., Di Diego, J.M., Zygmunt, A.C., Belardinelli, L., and Antzelevitch, C. (2007). Atrium-selective sodium channel block as a strategy for suppression of atrial fibrillation: differences in sodium channel inactivation between atria and ventricles and the role of ranolazine. Circulation *116*, 1449-1457.

Butterworth, J.F.t., and Strichartz, G.R. (1990). Molecular mechanisms of local anesthesia: a review. Anesthesiology *72*, 711-734.

Camm, A.J., and Lau, C.P. (2003). Electrophysiological effects of a single intravenous administration of ivabradine (S 16257) in adult patients with normal baseline electrophysiology. Drugs in R&D *4*, 83-89.

Chan, C.S., Shigemoto, R., Mercer, J.N., and Surmeier, D.J. (2004). HCN2 and HCN1 channels govern the regularity of autonomous pacemaking and synaptic resetting in globus pallidus neurons. J Neurosci *24*, 9921-9932.

Chen, S., Wang, J., Zhou, L., George, M.S., and Siegelbaum, S.A. (2007). Voltage sensor movement and cAMP binding allosterically regulate an inherently voltage-independent closed-open transition in HCN channels. The Journal of General Physiology *129*, 175-188.

Cheng, L., Kinard, K., Rajamani, R., and Sanguinetti, M.C. (2007). Molecular mapping of the binding site for a blocker of hyperpolarization-activated, cyclic nucleotide-modulated pacemaker channels. The Journal of Pharmacology and Experimental Therapeutics *322*, 931-939.

Demontis, G.C., Moroni, A., Gravante, B., Altomare, C., Longoni, B., Cervetto, L., and DiFrancesco, D. (2002). Functional characterisation and subcellular localisation of HCN1 channels in rabbit retinal rod photoreceptors. The Journal of Physiology *542*, 89-97.

DiFrancesco, D. (1993). Pacemaker mechanisms in cardiac tissue. Annual Review of Physiology *55*, 455-472.

DiFrancesco, D., and Borer, J.S. (2007). The funny current: cellular basis for the control of heart rate. Drugs *67 Suppl 2*, 15-24.

DiFrancesco, D., and Camm, J.A. (2004). Heart rate lowering by specific and selective I_f current inhibition with ivabradine: a new therapeutic perspective in cardiovascular disease. Drugs *64*, 1757-1765.

DiFrancesco, D., Ferroni, A., Mazzanti, M., and Tromba, C. (1986). Properties of the hyperpolarizing-activated current I_f in cells isolated from the rabbit sino-atrial node. The Journal of Physiology *377*, 61-88.

Galer, B.S., Rowbotham, M.C., Perander, J., and Friedman, E. (1999). Topical lidocaine patch relieves postherpetic neuralgia more effectively than a vehicle topical patch: results of an enriched enrollment study. Pain *80*, 533-538.

Gasparini, S., and DiFrancesco, D. (1997). Action of the hyperpolarization-activated current (I_h) blocker ZD 7288 in hippocampal CA1 neurons. Pflugers Arch *435*, 99-106.

Gauss, R., Seifert, R., and Kaupp, U.B. (1998). Molecular identification of a hyperpolarization-activated channel in sea urchin sperm. Nature *393*, 583-587.

Goodman, L.S., Hardman, J.G., Limbird, L.E., and Gilman, A.G. (2001). Goodman and Gilman's the pharmacological basis of therapeutics, 10th edn (New York, McGraw-Hill, Medical Pub. Division).

Grafe, P., Quasthoff, S., Grosskreutz, J., and Alzheimer, C. (1997). Function of the hyperpolarization-activated inward rectification in nonmyelinated peripheral rat and human axons. Journal of Neurophysiology *77*, 421-426.

Grant, A.O., Strauss, L.J., Wallace, A.G., and Strauss, H.C. (1980). The influence of pH on the electrophysiological effects of lidocaine in guinea pig ventricular myocardium. Circulation Research *47*, 542-550.

Harris, N.C., and Constanti, A. (1995). Mechanism of block by ZD 7288 of the hyperpolarization-activated inward rectifying current in guinea pig substantia nigra neurons in vitro. Journal of Neurophysiology *74*, 2366-2378.

Harrison, D.C., and Collinsworth, K.A. (1974). Antiarrhythmic actions of lidocaine. Annual Review of Medicine *25*, 143-148.

Heavner, J.E. (2007). Local anesthetics. Current Opinion in Anaesthesiology *20*, 336-342.

Heginbotham, L., and Kutluay, E. (2004). Revisiting voltage-dependent relief of block in ion channels: a mechanism independent of punchthrough. Biophysical Journal *86*, 3663-3670.

Heginbotham, L., and MacKinnon, R. (1992). The aromatic binding site for tetraethylammonium ion on potassium channels. Neuron *8*, 483-491.

Hille, B. (1977a). Local anesthetics: hydrophilic and hydrophobic pathways for the drug-receptor reaction. The Journal of General Physiology *69*, 497-515.

Hille, B. (1977b). The pH-dependent rate of action of local anesthetics on the node of Ranvier. The Journal of General Physiology *69*, 475-496.

Hille, B. (2001). Ion channels of excitable membranes, 3rd edn (Sunderland, Mass., Sinauer).

Hondeghem, L.M., and Katzung, B.G. (1977). Time- and voltage-dependent interactions of antiarrhythmic drugs with cardiac sodium channels. Biochimica et Biophysica Acta *472*, 373-398.

Ishii, T.M., Nakashima, N., Takatsuka, K., and Ohmori, H. (2007). Peripheral N- and C-terminal domains determine deactivation kinetics of HCN channels. Biochemical and Biophysical Research Communications *359*, 592-598.

Kilb, W., and Luhmann, H.J. (2000). Characterization of a hyperpolarization-activated inward current in Cajal-Retzius cells in rat neonatal neocortex. Journal of Neurophysiology *84*, 1681-1691.

Kindler, C.H., and Yost, C.S. (2005). Two-pore domain potassium channels: new sites of local anesthetic action and toxicity. Regional Anesthesia and Pain Medicine *30*, 260-274.

Komai, H., and McDowell, T.S. (2001). Local anesthetic inhibition of voltage-activated potassium currents in rat dorsal root ganglion neurons. Anesthesiology *94*, 1089-1095.

Ludwig, A., Budde, T., Stieber, J., Moosmang, S., Wahl, C., Holthoff, K., Langebartels, A., Wotjak, C., Munsch, T., Zong, X., *et al.* (2003). Absence epilepsy and sinus dysrhythmia in mice lacking the pacemaker channel HCN2. The EMBO Journal *22*, 216-224.

Ludwig, A., Zong, X., Jeglitsch, M., Hofmann, F., and Biel, M. (1998). A family of hyperpolarization-activated mammalian cation channels. Nature *393*, 587-591.

Luthi, A., and McCormick, D.A. (1998). H-current: properties of a neuronal and network pacemaker. Neuron *21*, 9-12.

Mayer, M.L., and Westbrook, G.L. (1983). A voltage-clamp analysis of inward (anomalous) rectification in mouse spinal sensory ganglion neurones. The Journal of Physiology *340*, 19-45.

Momin, A., Cadiou, H., Mason, A., and McNaughton, P.A. (2008). Role of the hyperpolarization-activated current I_h in somatosensory neurons. The Journal of Physiology *586*, 5911-5929.

Moosmang, S., Stieber, J., Zong, X., Biel, M., Hofmann, F., and Ludwig, A. (2001). Cellular expression and functional characterization of four hyperpolarization-activated pacemaker channels in cardiac and neuronal tissues. European Journal of Biochemistry / FEBS *268*, 1646-1652.

Nolan, M.F., Malleret, G., Lee, K.H., Gibbs, E., Dudman, J.T., Santoro, B., Yin, D., Thompson, R.F., Siegelbaum, S.A., Kandel, E.R., *et al.* (2003). The hyperpolarization-activated HCN1 channel is important for motor learning and neuronal integration by cerebellar Purkinje cells. Cell *115*, 551-564.

Olschewski, A., Brau, M.E., Olschewski, H., Hempelmann, G., and Vogel, W. (1996). ATP-dependent potassium channel in rat cardiomyocytes is blocked by lidocaine. Possible impact on the antiarrhythmic action of lidocaine. Circulation 93, 656-659.

Olschewski, A., Hempelmann, G., Vogel, W., and Safronov, B.V. (1998). Blockade of Na^+ and K^+ currents by local anesthetics in the dorsal horn neurons of the spinal cord. Anesthesiology 88, 172-179.

Pape, H.C. (1996). Queer current and pacemaker: the hyperpolarization-activated cation current in neurons. Annual Review of Physiology 58, 299-327.

Pape, H.C., and McCormick, D.A. (1989). Noradrenaline and serotonin selectively modulate thalamic burst firing by enhancing a hyperpolarization-activated cation current. Nature 340, 715-718.

Perkins, K.L., and Wong, R.K. (1995). Intracellular QX-314 blocks the hyperpolarization-activated inward current I_q in hippocampal CA1 pyramidal cells. Journal of Neurophysiology 73, 911-915.

Pian, P., Bucchi, A., Robinson, R.B., and Siegelbaum, S.A. (2006). Regulation of gating and rundown of HCN hyperpolarization-activated channels by exogenous and endogenous PIP_2. The Journal of General Physiology 128, 593-604.

Proenza, C., Angoli, D., Agranovich, E., Macri, V., and Accili, E.A. (2002). Pacemaker channels produce an instantaneous current. The Journal of Biological Chemistry 277, 5101-5109.

Robinson, R.B., and Siegelbaum, S.A. (2003). Hyperpolarization-activated cation currents: from molecules to physiological function. Annual Review of Physiology 65, 453-480.

Rocchetti, M., Armato, A., Cavalieri, B., Micheletti, M., and Zaza, A. (1999). Lidocaine inhibition of the hyperpolarization-activated current (I_f) in sinoatrial myocytes. Journal of Cardiovascular Pharmacology 34, 434-439.

Santoro, B., Liu, D.T., Yao, H., Bartsch, D., Kandel, E.R., Siegelbaum, S.A., and Tibbs, G.R. (1998). Identification of a gene encoding a hyperpolarization-activated pacemaker channel of brain. Cell 93, 717-729.

Shi, W., Wymore, R., Yu, H., Wu, J., Wymore, R.T., Pan, Z., Robinson, R.B., Dixon, J.E., McKinnon, D., and Cohen, I.S. (1999). Distribution and prevalence of hyperpolarization-activated cation channel (HCN) mRNA expression in cardiac tissues. Circulation Research 85, e1-6.

Shin, K.S., Rothberg, B.S., and Yellen, G. (2001). Blocker state dependence and trapping in hyperpolarization-activated cation channels: evidence for an intracellular activation gate. The Journal of General Physiology 117, 91-101.

Takigawa, T., Alzheimer, C., Quasthoff, S., and Grafe, P. (1998). A special blocker reveals the presence and function of the hyperpolarization-activated cation current I_h in peripheral mammalian nerve fibres. Neuroscience *82*, 631-634.

Tamura, A., Ogura, T., Uemura, H., Reien, Y., Kishimoto, T., Nagai, T., Komuro, I., Miyazaki, M., and Nakaya, H. (2009). Effects of Antiarrhythmic Drugs on the Hyperpolarization-Activated Cyclic Nucleotide-Gated Channel Current. Journal of Pharmacological Sciences. *110*, 150-159.

Thollon, C., Cambarrat, C., Vian, J., Prost, J.F., Peglion, J.L., and Vilaine, J.P. (1994). Electrophysiological effects of S 16257, a novel sino-atrial node modulator, on rabbit and guinea-pig cardiac preparations: comparison with UL-FS 49. British Journal of Pharmacology *112*, 37-42.

Tu, H., Deng, L., Sun, Q., Yao, L., Han, J.S., and Wan, Y. (2004). Hyperpolarization-activated, cyclic nucleotide-gated cation channels: roles in the differential electrophysiological properties of rat primary afferent neurons. Journal of Neuroscience Research *76*, 713-722.

Ulens, C., and Tytgat, J. (2001). Functional heteromerization of HCN1 and HCN2 pacemaker channels. The Journal of Biological Chemistry *276*, 6069-6072.

Woodhull, A.M. (1973). Ionic blockage of sodium channels in nerve. The Journal of General Physiology *61*, 687-708.

Yagi, J., and Sumino, R. (1998). Inhibition of a hyperpolarization-activated current by clonidine in rat dorsal root ganglion neurons. Journal of Neurophysiology *80*, 1094-1104.

APPENDICES

Appendix 1.

Figure A1.1. 200 μM lidocaine inhibits I_f at -110 mV with complete current return. (Top) Current traces showing the effects of control (a), perfusion of 200 μM lidocaine for 2.5 minutes (b), and 2.5 minutes following drug removal from bath (c). Protocol is shown in the inset to the right. (Bottom) Time-dependent current (I_f) plotted over time. Note that current traces and recordings of I_f are obtained every 12 seconds. Complete washout is observed, as currents return to the level prior to lidocaine addition.
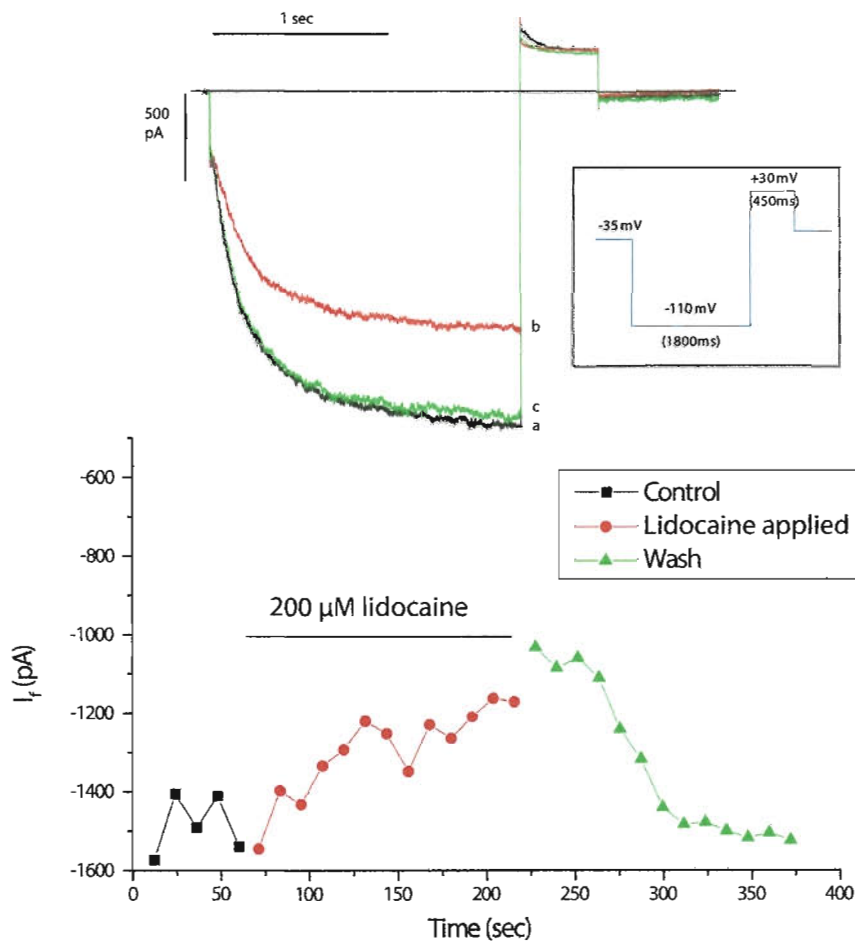
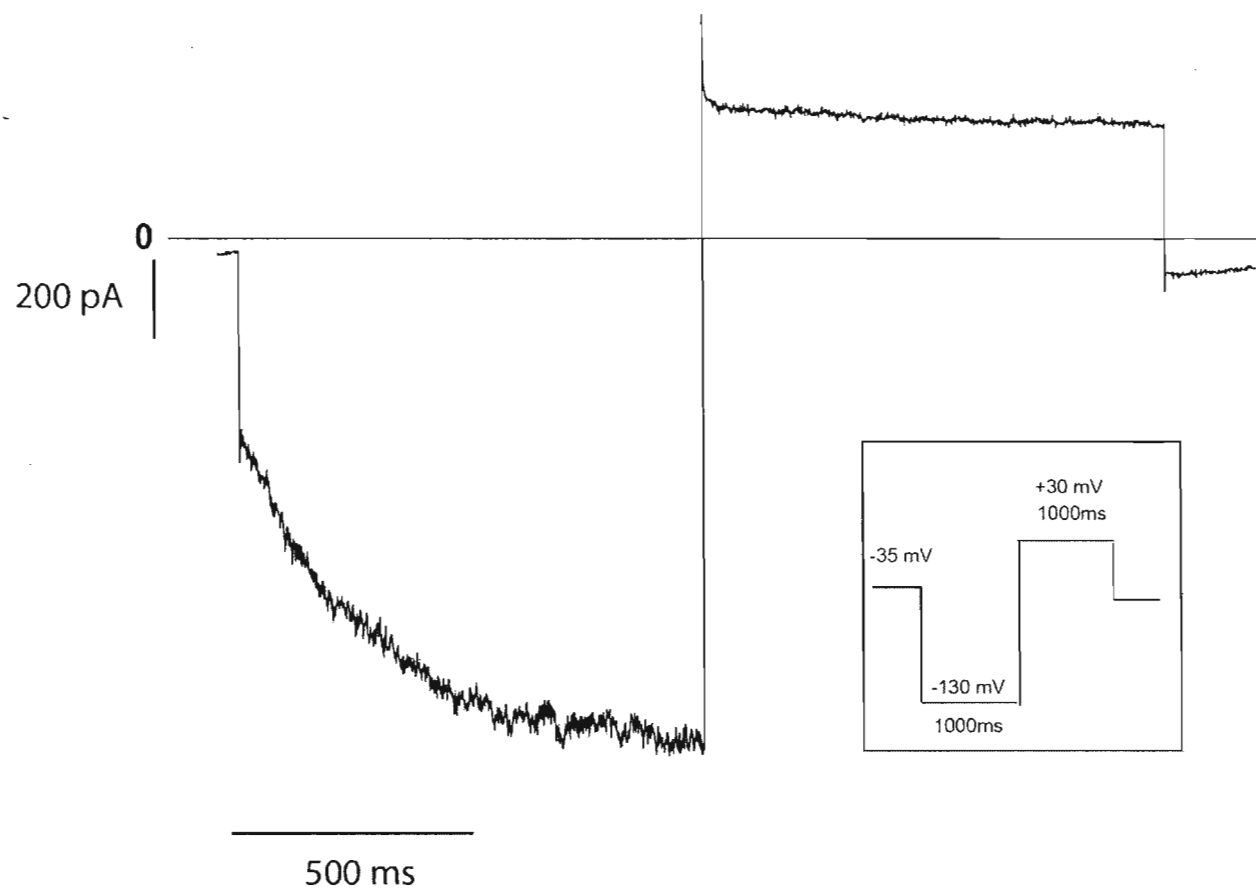**Appendix 2.**

Figure A2.1. Representative current trace of HCN1 A372G.

Figure A2.2. Representative current trace of HCN1 V379A.